

Christoph Trenk, BSc

Role of miR-3150b-3p and miR-4521 in breast carcinogenesis

Master's Thesis

To achieve the university degree of

Master of Science

Master's degree programme: Biochemistry and Molecular Biomedical Sciences

submitted to

Medical University of Graz

Supervisor

Assoz. Prof. Priv.-Doz. Dr.med.univ. Martin Pichler

Division of Oncology

Research Unit for Non-coding RNAs and Genome Editing in Cancer

January 2019

Affidavit

I declare that I have authored this thesis independently, that I have not used other than the declared sources/resources, and that I have explicitly indicated all material which has been quoted either literally or by content from the sources used.

The text document uploaded to TUGRAZonline is identical to the present master's thesis.

Date

Signature

Danksagung

Als erstes möchte ich mich an dieser Stelle bei allen bedanken, die mir während der Masterarbeit im Labor zur Seite gestanden sind und mich unterstützt haben.

Ein besonderer Dank gilt Martin Pichler, der mir mit seinem Wissen und seiner Expertise immer wieder weitergeholfen hat in Zeiten wo ich eine gute Betreuung benötigt habe. Außerdem konnte ich mich durch seinen Stil zum selbstständigen Arbeiten motivieren und mich weiterentwickeln.

Ebenfalls bedanke ich mich bei Felix, Christiane und Margit, zu denen ich auch mit meinen Fragen kommen durfte und immer ein offenes Ohr fand. Außerdem wurde ich von ihnen und den anderen im Labor von Anfang an herzlich in die Gruppe aufgenommen was zu einem sehr guten Arbeitsklima führte.

Zusätzlich haben mir meine StudienkollegInnen während des gesamten Masters die Studienzeit mit zahllosen Unternehmungen versüßt. Dadurch konnte ich regelmäßig abschalten und mich mit neuer Energie wieder an die Arbeit machen.

Nun möchte ich mich noch bei meiner Familie bedanken. Meine Eltern haben mich über all die Jahre nicht nur finanziell, sondern auch seelisch unterstützt. Zusätzlich haben mein Bruder Dominik und all meine Freunde aus Ried im Innkreis an den Wochenenden außerhalb von Graz für den nötigen Spaß gesorgt. Ebenfalls sorgte mein bester Freund Raphael mit Brettspielabenden für den nötigen Ausgleich.

Am Ende gilt noch ein ganz besonderer Dank meiner Freundin Sandra. Sie hat sich während der ganzen Zeit unterstützt und ist mir zur Seite gestanden, wann mir der nötige Halt fehlte.

Abstract

MicroRNAs are small non-coding RNAs that are known to be key regulators in basic biological processes not only in normal cells but especially in cancerous cells. Additionally, particularly miR-4521 has been found to be upregulated whereas miR-3150b-3p seemed to be downregulated in patients' breast cancer tissues compared to normal breast tissues. However, their role in the initiation and progression in cancer is not known yet. Therefore, the aim of this study was to characterize and elucidate the functions of these microRNAs in triple negative breast cancer.

For this, the triple negative breast cancer cell lines BT-549, MDA-MB-231 and SUM159 were used for all experiments. I firstly transiently transfected these cell lines with miR-4521 and miR-3150b-3p mimics and inhibitors. In the next steps, I analyzed if there is an effect on different hallmarks of cancer with a special focus on proliferation and angiogenesis. After showing that a significant up- and downregulation of miR-4521 and miR-3150b-3p can be achieved in my experimental model system, I found that the mimic led to an increase in proliferation, whereas the inhibitor demonstrated the opposite effect. These results were confirmed in a colony formation unit assay where the inhibitor led to the formation of significantly less colonies while the mimics showed an increase. In the case of miR-3150b-3p also the inhibitor resulted in a slight increase in proliferation and the mimic seemed to inhibit colony formation. Moreover, it has been shown that miR-4521 overexpression led to a higher number of tubes in the tube formation assay in human endothelial cells. Again, the inhibition resulted in the opposite results.

Altogether, these data suggest that miR-4521 plays an important role in cellular growth as well as angiogenesis and might act as tumour suppressor in triple negative breast cancer. Contrary, the role of miR-3150b-3p needs to be further investigated as the results are contradictory.

Zusammenfassung

MikroRNAs sind kleine nicht-codierende RNAs, die für ihre Rolle als Schlüsselregulatoren in grundlegenden biologischen Prozessen in gesunden Zellen und besonders in Tumorzellen, bekannt sind. Frühere Arbeiten konnten zeigen, dass miR-4521 in Brustkrebsgewebe von Patienten hochreguliert und miR-3150b-3p hingegen runterreguliert ist. Jedoch ist deren Rolle bei der Ausbildung und Progression von Krebs noch nicht bekannt. Deswegen war das Ziel dieser Arbeit die Funktionen dieser beiden mikroRNAs in triple negativem Brustkrebs zu charakterisieren.

Dafür wurden die triple negativen Brustkrebszelllinien BT-549, MDA-MB-231 und SUM159 für alle Experimente verwendet und mit miR-4521 und miR-3150b-3p Mimics und Inhibitoren transfiziert. Im nächsten Schritt wurde analysiert, ob sie einen Effekt auf die beiden Hallmarks of Cancer Proliferation und Angiogenese haben. Nachdem nachgewiesen wurde, dass die Expression von miR-4521 und miR-3150b-3p erfolgreich überexprimiert beziehungsweise gehemmt werden kann, konnte ich zeigen, dass das miR-4521 Mimic zu einer Steigerung der Proliferation führt während der Inhibitor das Gegenteil zur Folge hat. Die Ergebnisse wurden im Colony forming unit Assay bestätigt, in dem der Inhibitor zur Bildung von signifikant weniger Kolonien führte während das Mimic zu einer erhöhten Kolonienzahl führte. Im Falle der miR-3150b-3p führte der Inhibitor zu einer geringen Steigerung des Zellwachstums und das Mimic hat die Bildung von Kolonien inhibiert. Weiters wurde gezeigt, dass eine erhöhte Expression der miR-4521 zu einer höheren Anzahl an Gefäßen im Tube formation Assay in humanen Endothelzellen führte. Wieder ergab die Inhibition gegensätzliche Ergebnisse.

Zusammengefasst, deuten diese Daten darauf hin, dass miR-4521 eine wichtige Rolle in Proliferation und Angiogenese spielt und möglicherweise als Tumorsuppressor in triple negativem Brustkrebs wirkt. Im Gegensatz dazu sollte die miR-3150b-3p noch weiter untersucht werden, da die Ergebnisse widersprüchliches zeigen.

Table of contents

Affidavit	i
Danksagung	ii
Abstract.....	iii
Zusammenfassung	iv
1 Introduction	1
1.1 Breast cancer	2
1.1.1 Incidence	2
1.1.2 Intrinsic molecular subtypes	3
1.2 Proliferation.....	5
1.3 Apoptosis	10
1.4 Angiogenesis.....	12
1.4.1 MicroRNAs.....	13
1.5 Aim of this study.....	18
2 Materials.....	19
2.1 Cell culture.....	20
2.2 Transfection	21
2.2.1 Reagents.....	21
2.2.2 MiRNA mimics and inhibitors.....	21
2.3 RNA purification.....	22
2.4 CDNA synthesis.....	22
2.5 Real-time qPCR	23
2.5.1 Kit.....	23
2.5.2 Primer.....	23
2.6 WST-1 metabolic proliferation assay.....	24

2.7	Colony forming unit assay	24
2.8	Cell cycle analysis.....	24
2.9	Apoptosis assay	25
2.10	<i>In vitro</i> angiogenesis assay.....	25
3	Equipment	26
4	Methods	28
4.1	<i>In silico</i> analysis.....	29
4.1.1	Overall survival analysis	29
4.1.2	Housekeeping gene analysis	29
4.2	Cell culture.....	29
4.3	Fast-forward transfection.....	30
4.4	Reverse transfection.....	32
4.5	Purification of total RNA.....	32
4.6	CDNA synthesis.....	33
4.7	Real-time qPCR	34
4.8	WST-1 metabolic proliferation assay.....	36
4.9	Colony forming unit assay	36
4.10	Cell cycle analysis	37
4.11	Apoptosis assay.....	38
4.12	<i>In vitro</i> angiogenesis assay.....	38
5	Results	39
5.1	<i>In silico</i> analysis.....	40
5.1.1	Overall survival regarding expression of miR-3150b-3p and miR-4521	40
5.1.2	Determination of a stable housekeeping gene	41
5.2	Expression analysis of miRNAs in different breast cancer cell lines.....	42
5.3	Manipulation of miRNA expression levels using mimics and inhibitors	44

5.4	Effect of miRNA mimics and inhibitors on proliferation	46
5.5	Differences in colony formation in transfected breast cancer cell lines.....	49
5.6	Influence of miR-4521 on cell cycle progression in BT-549.....	50
5.7	Stimulation of apoptosis in TNBC cell lines	52
5.8	Expression levels of two cell cycle markers under the influence of miR-4521	53
5.9	MiR-3150b-3p and miR-4521 influence tube formation in HUVEC.....	54
5.10	Angiogenesis related gene expression influenced by miR-4521	56
6	Discussion	58
	Abbreviations	viii
	References.....	xi

1 Introduction

1.1 Breast cancer

1.1.1 Incidence

Breast cancer has the highest number of diagnoses and is the leading cause of cancer death amongst women worldwide. GLOBOCAN estimated that for all cancer types combined there would be 18.1 million new cases and 9.6 million cancer deaths worldwide in 2018. Amongst these, breast cancer alone was predicted to account for 11.6 % of new cases and 6.6 % of deaths and is therefore regarded as the most prevalent cancer type in most countries (Bray et al. 2018).

While cancer in general, is a global rapidly growing disease (Bray et al. 2018), breast cancer incidence rates were relatively stable in Austria from 1996 to 2016. Moreover, the number of deaths decreased by 13 % over the years (<http://www.statistik-austria.at>; December 25.2019). This is due to a better accessibility to screening and therapeutic programs (Momenimovahed et al. 2019). However, with 5,558 new cases of which 1,588 resulted in death, breast cancer accounted for 17 % of all cancer deaths in 2016 and therefore was the one with the highest mortality of all cancer types amongst women (<http://www.statistik-austria.at>; December 25.2019).

Differences in breast cancer development can not only be observed in Austria but in countries all over the world depending on various circumstances. Incidence is commonly higher in developed countries by virtue of an increased prevalence of known risk factors such as higher age, exogenous hormone intake, oral contraceptive pills and hormone replacement therapy. Additionally, factors such as, nutrition and lifestyle leaning towards excessive alcohol intake and smoking, and obesity attended by high insulin levels or insulin-like factors stimulate the growth of cancer cells. Furthermore, nulliparity, late age at first birth, and fewer children constitute a higher risk of developing breast cancer, whereas breastfeeding as well as physical activity count as protective factors. Therefore, the increased incidence in higher human development index countries (HDI) reflects a

combination of all these social and economic factors (Bray et al. 2018, Momenimovahed et al. 2019).

1.1.2 Intrinsic molecular subtypes

Breast cancer can be classified into four main intrinsic molecular subtypes: luminal A, luminal B, HER2/neu-enriched, and basal-like including triple negative (TNBC) subtype. Each of these subtypes reflects a distinct expression pattern of signature genes for hormone receptors (HR) (estrogen (ER) and progesterone receptor (PR)), human epidermal growth factor receptor (HER2/neu), proliferation-related genes and many more. Additionally, this characterization on RNA and protein level allows a closer selection of the adequate therapy, and the prediction of treatment response and prognosis (American Cancer Society. Breast Cancer Facts & Figures 2017-2018. Atlanta: American Cancer Society, Inc. 2017, Prat et al. 2015).

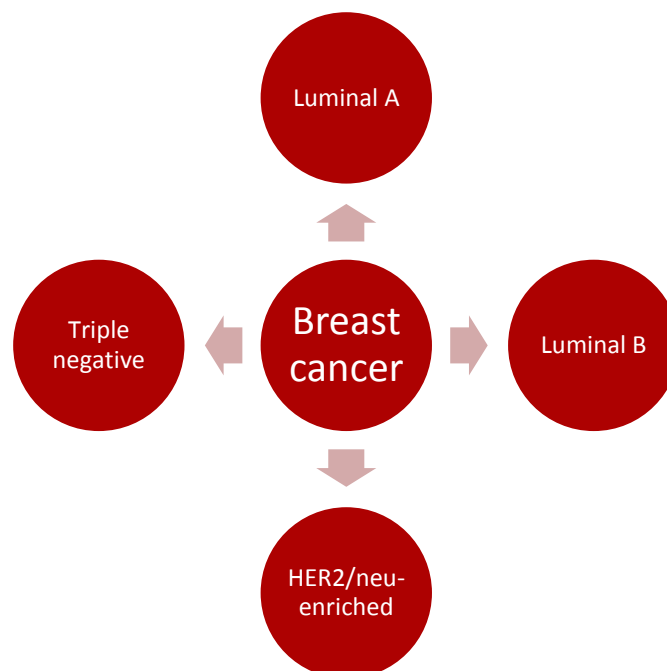


Figure 1: Intrinsic molecular subtypes of breast cancer. Dependent on the expression pattern of HRs and HER2/neu, breast cancer can be classified into four main intrinsic subtypes luminal A, luminal B, HER2/neu-enriched and triple negative.

The luminal A subtype is distinguished by its expression of the ER, a variable expression of the PR and its lack of the HER2/neu expression. These tumors represent 71% of all subtypes

and are known to proliferate slowly and show less aggressiveness than others. Additionally, prognosis is most beneficial because of a high response to anti-hormone treatment (American Cancer Society. Breast Cancer Facts & Figures 2017-2018. Atlanta: American Cancer Society, Inc. 2017).

Another class of breast cancer called luminal B is –similar to luminal A- defined by its expression of ER as well as PR, but it also displays HER2/neu positivity. Unfortunately, this subtype shows worse prognosis in terms of recurrence and metastasis. However, both luminal A and luminal B respond to endocrine therapies (American Cancer Society. Breast Cancer Facts & Figures 2017-2018. Atlanta: American Cancer Society, Inc. 2017, Li et al. 2016).

Tamoxifen is used as standard adjuvant therapy in early and advanced ER-positive breast cancer and displays the least toxicity amongst other regimens. It acts by inhibiting the entry of estrogen into cells, thus inhibiting cell growth and proliferation (Akram et al. 2017). Moreover, aromatase inhibitors constitute another treatment possibility for these subtypes of breast cancer in postmenopausal women (American Cancer Society. Breast Cancer Facts & Figures 2017-2018. Atlanta: American Cancer Society, Inc. 2017). Aromatase is an enzyme complex that performs the last step in estrogen biosynthesis and as a result depletes tumour cells of this hormone (Akram et al. 2017).

Besides HR positive breast cancer there are also subtypes that lack the expression of ER and PR. One of these is characterized by HER2/neu upregulation and therefore is called HER2/neu-enriched. It carries the highest number of genomic mutations resulting in faster growth and dissemination. Though, risk of recurrence and death are decreased by 52% and 33% respectively, mainly due to Trastuzumab. Trastuzumab is a monoclonal antibody which directly targets the HER2/neu receptor. (American Cancer Society. Breast Cancer Facts & Figures 2017-2018. Atlanta: American Cancer Society, Inc. 2017, Prat et al. 2015)

The fourth subtype, TNBC, is known to be the most aggressive and the least treatable subtype. Tumour cells of this subtype are deficient in ER, PR, and HER2/neu expression and therefore provide no targets for hormonal and anti-HER2/neu therapy. For this reason, the standard treatment is still chemotherapy based on anthracycline/taxane (Schneeweiss A. et al. 2019). Moreover, TNBC is generally associated with very short recurrence free survival and displays a tremendous risk of metastasis (Aysola K. et al. 2013). Notably, these aggressive tumors are more often found in African and younger women (Bray et al. 2018).

1.2 Proliferation

Proliferation describes the fundamental process in which cells undergo various phases of the cell-cycle to successfully divide into two genetically identical daughter cells. The phases can be divided into G phases (G for gap), where cells grow and double the amount of proteins and organelles, the S phase (S for synthesis) in which the great amount of DNA is duplicated and finally the M phase (M for mitosis) where one mother cells is divided into two new daughter cells by cytokinesis. For this, all the produced components and the DNA in form of chromosomes need to be split equally in the last phase. Afterwards, the cycle can be repeated. However, if and when proliferation is executed is strongly regulated by the cell-cycle control system dependent on cyclin-dependent kinases (Cdks) (Alberts et al. 2015, Lodish et al. 2012).

As the name suggests, the activity of these Cdks is dependent on binding of cyclins. Serine/threonine kinase activity is switched on via binding of cyclins to their interaction partners. First, Cdks undergo a conformational change whereby the active site is accessible for the Cdk-activating kinase (CAK) that lead to their full activation by phosphorylation of an activating threonine in the active side. As a result, target substrate proteins can be phosphorylated and thereby activated (Alberts et al. 2015, Lodish et al. 2012). Besides enzymes such as Cdk inhibitor proteins, ubiquitin ligases, and phosphatases, there are four major classes of cyclins of which three are crucial for the regulation of the cell cycle. These enzymes are not simply specific for distinct Cdks but additionally expressed only in the phase they are responsible for. Afterwards, they are degraded again until the next cycle starts.

Hence, G₁/S-cyclins are expressed in the late G₁ mediated by G₁-cyclins, S-cyclins abundance is high through S and G₂, and the expression levels of M-cyclins rise in G₂ and are at their peak in the first half of M. Altogether, these cyclins bound to their partner Cdks initiate the progression through the phases of the cell cycle (Alberts et al. 2015, Bertoli et al. 2013, Murray 2004). Yet, mammalian cells undergo this process only when the first of three main regulatory transitions is accomplished and when the environment in- and outside the cell is favorable throughout the phases (Alberts et al. 2015, Bertoli et al. 2013).

The first transition at the end of G₁ by which the cell cycle is initiated is called restriction point. After reaching this point of no return, cells are not only committed to proliferation, but also to initiation of DNA synthesis (Alberts et al. 2015). Upon mitogenic signalling via the Ras/Raf/mitogen-activated protein kinase (MAPK) pathway cyclin D (D1, D2, and D3) is expressed and interacts with the G₁-Cdks (Cdk4 and Cdk6). In this manner, D-type cyclins function as growth factor sensors and furthermore phosphorylate retinoblastoma protein (Rb). In this step inhibitors of Cdk4 (INK4) proteins, namely p16^{INK4a}, p15^{INK4b}, p18^{INK4c}, and p19^{INK4d} come into play targeting cyclin D-Cdk4 and -Cdk6 interaction causing G₁ arrest. In the case of G₁ progression, the G₁/S-cyclin (cyclin E) is activated and binds to its target Cdk2 leading to hyperphosphorylation of Rb. This results in the inhibition of its suppressing properties on the E2F transcription factor family. Then, expressed E2F-regulated genes such as cyclin E, and cyclin A (S-cyclin) with their interaction partners Cdk2 and 1, drive cells into S phase (Sherr & Roberts 2019, Duronio & Xiong 2013). Inhibitors of the Cip/Kip family such as p21^{Cip1} and p27^{Kip1} negatively influence cyclin D-, E-, and A-dependent kinases in order to block phosphorylation by CAK (Aprelikova et al. 1995) resulting in cell cycle arrest. P21^{Cip1} blocks chromosome duplication in the presence of DNA damage and p27^{Kip1} in turn is implicated in a positive feedback loop of G₁/S-Cdks in which active Cdk2 marks this protein with a phosphate for degradation by the ubiquitin-protein ligase SCF (Skp1, Cullin, F-box proteins) (Alberts et al. 2015, Duronio & Xiong 2013, Lodish et al. 2012). By doing so, the cells fate is determined and DNA synthesis is executed without further exterior stimulation needed (Sherr & Roberts 2019).

Replication during S needs numerous preparation steps already in the course of G₁ to finally ensure proper DNA duplication throughout the whole process (Moiseeva & Bakkenist 2018). In eukaryotes replication starts at origins of replication which are recognized by a complex formed by six proteins in an ATP-dependent manner (ORC1-6) (Siddiqui & Stillman 2007, Bell & Stillman 1992). Afterwards, the pre-replication complex (pre-RC) is formed beginning with the recruitment of the cell division cycle 6 (Cdc6) protein required for the loading of the minichromosome maintenance (MCM) heterohexamer (MCM2-7). During this time chromatin licensing and DNA replication factor 1 (Cdt1) is associated to the ring-shaped MCM complex stabilizing an open state for DNA channeling (Frigola et al. 2016) and these together forming the pre-RC. From this point on S-Cdks and other enzymes throw the switch initiating S phase (Alberts et al. 2015).

Therefore, a sequence of multiple protein recruiting steps lead to the synthesis of two exact copies of the original chromosomes. For this, phosphorylation of the MCM complex by Cdc7-DBF4/DBF4-dependent kinase (DDK) is crucial for the interaction with the firing factors (induce replication at origins of replication), Cdc45 and GINS (CMG complex) to further function as helicase (Bryant & Aves 2011). Additional essential factors such as DNA polymerases δ and ϵ , topoisomerase II, replication protein A, and primase are recruited with the contribution of DDK and S-Cdks. Together they trigger formation of the replication fork and elongation of the daughter DNA strands (Lodish et al. 2012, Yeeles et al. 2015). The two sister chromatids are held together via cohesins which is of great importance for their separation during M phase. Accordingly, the cell can enter the second main regulatory transition called G₂/M transition (Alberts et al. 2015).

Only if chromosome replication was successful the cell-cycle control system triggers the entry into M. During interphase (G₁, S, G₂) synthesis of M-Cdk, the complex of cyclin B (M-cyclin) and its interaction partner Cdk1, increases and peaks at the end of G₂. However, these complexes are rendered inactive by inhibitory phosphorylation due to the protein kinase Wee1. Upon stimulation favorable conditions the inhibitory phosphates are removed by protein phosphatase Cdc25 and M-Cdk induces mitosis including five stages called prophase, prometaphase, metaphase, anaphase, and telophase. In prophase chromosome

condensation and sister-chromatid resolution occurs leading to compact chromosomes and separable sister-chromatids. For this, M-Cdk phosphorylates condensin which changes DNA coiling. At the same time, centrosome replication is completed. Subsequently, each of the two centrosomes moves to its pole of the mitotic spindle with the help of microtubules and the motor proteins dynein, kinesin-5, and -14. At the beginning of prometaphase nuclear envelope breakdown is triggered rapidly. Moreover, astral microtubules attach the centrosomes to the cell cortex, interpolar and kinetochore microtubules extend to the middle of the cell while former interact with interpolar microtubules from the opposite pole and latter bind to opposing kinetochores (bi-orientation) at the centromere of each sister chromatid. In addition, two protein classes namely Aurora-A and Polo-like kinases are implicated in centrosome separation and kinetochore-microtubule interaction. Finally, when bi-orientated attachment of the kinetochores of every chromosome and their localization in the metaphase plate between the two spindle poles was successful in metaphase, the last main transition can be started (Alberts et al. 2015).

At the metaphase-to-anaphase transition a new complex comes into play regulating sister-chromatid separation. The anaphase-promoting complex or cyclosome (APC/C) belongs to the same family of enzymes like the SCF important for S induction. The APC/C is activated by M-Cdk promoted Cdc20 activity and targets a protein called securin that holds the enzyme separase in an inactive state via binding to it. The ubiquitinylation of securin leads to its degradation and activation of separase. As a result, cohesins holding sister-chromatids together are cleaved and mitotic cells undergo chromosome segregation in anaphase A and B. In anaphase A the kinetochore microtubules are shortened at the plus-end facing the kinetochore and depolymerization of the minus-end directed to the poles both ensuring the movement of the chromosomes towards these. During anaphase B the spindle poles themselves are pushed apart by kinesin-5 motor proteins on the interpolar microtubules and torn to the opposite sites of the cell by dynein anchored to the astral microtubules. As a result, the daughter chromosomes are split equally and can be packaged into two identical daughter nuclei in telophase followed by cytokinesis resulting in the succession of mitosis (Alberts et al. 2015).

For the last two steps, the APC/C arranges S- and M-Cdk destruction already in anaphase for the intracellular environment to re-form again. The dephosphorylation of Cdk targets makes it possible that fragments of the nuclear envelope interact with the surface of the chromosomes and fuse again to an intact membrane. Additionally, the endoplasmatic reticulum is re-built and forms the continuous organelle with the nucleus. Furthermore, pore complexes import nuclear proteins that lead to expansion of the nucleus and relaxation of the chromosomes to their interphase structure. To complete the cell cycle, a structure consisting of actin and myosin II forms during anaphase. This round-shaped organization of filaments in the middle of the cell between the two daughter nuclei is called the contractile ring. A protein of the Ras superfamily, namely RhoA gets activated by the Rho-guanine nucleotide exchange factor (Rho-GEF). Subsequently, the stimulation of formin leads to actin filament formation, the Rho-activated kinases such as Rock execute regulatory myosin light-chain phosphorylation (motor activity) of myosin II. Both together lead to assembly and contraction of the round-shaped structure in the middle of the cell between the two daughter nuclei, namely the contractile ring. In this process, enough force is exerted to divide the cell into two daughter cells (Alberts et al. 2015). This highly regulated and complex but essential process, including a sequence of numerous protein-protein interactions, and a balance between activating as well as inhibitory events makes it possible for cells to proliferate. However, all the genes and proteins needed for the cell cycle constitute countless points for mutations leading to uncontrolled proliferative signalling.

Sustaining proliferative signalling is the most important hallmark of cancer. Cell cycle initiation depends on stimulation through extracellular signals and cancer cells can get hyperresponsive to growth factors by overexpression of associated receptors (Hanahan & Weinberg 2011). The Her2/neu receptor for example is overexpressed in breast cancer increasing receptor-dependent proliferative signalling (Witsch et al. 2010). Moreover, B-Raf a serine/threonine kinase in the Ras/Raf/MEK/ERK pathway downstream of growth factor receptors frequently shows mutations in human malignancies. These mutations lead to permanent activation of B-Raf followed by constitutive stimulation of downstream targets. Additionally, some aberrations in the gene lead to the loss of the kinase activity although resulting in increased signalling due to compensation via C-Raf, another oncogene (Wan et

al. 2004). However, also proteins directly involved in the cell cycle can be affected such as tumour suppressor p27. Loss of this Cdk inhibitor correlates with progression of TNBC in African American women (Khan et al. 2018). Altogether, it can be said that impaired proliferation is a key biological process across all cancer types. Moreover, resistance to apoptosis displays another hallmark of cancer supporting unlimited proliferation (Evan & Vousden 2001).

1.3 Apoptosis

Before cells accumulate irreparable DNA damages, or exhibit excessive levels of mitotic signalling both possibly leading to the development of tumorous behavior they undergo apoptosis. This mechanism of programmed cell death is designed to eliminate abnormal cells, or cells representing danger to the organism and hinder them from spreading mutations or cancerous traits throughout surrounding tissue (Evan & Littlewood 1998, Hanahan & Weinberg 2011). When unwanted cells or an unfavorable environment within a cell is sensed, apoptosis is initiated. It starts with nuclear and cytoplasmic condensation followed by the degradation of cellular proteins and DNA by the main enzymes of apoptosis, the caspases. Afterwards, plasma membrane blebbing occurs and cells are fragmented into small apoptotic bodies phagocytosed by surrounding cells. In the course of this controlled biological process no cytoplasmic leakage occurs by what tissue inflammation and damage to neighboring cells is prohibited. However, if and when apoptosis is executed depends on intra- and extracellular signals (Cairrão & Domingos 2010).

Activation of the intrinsic pathway is based on the formation of the apoptosome, a complex of multiple proteins. Before this multiprotein complex can be assembled, the pro-apoptotic B-cell lymphoma 2 (Bcl-2) homology (BH) 3-only domain proteins such as Bid are needed to inhibit the anti-apoptotic proteins including multiple BH domains, e.g. Bcl-2. Accordingly, another group of pro-apoptotic multidomain proteins like Bcl-2 associated X protein (Bax) are released upon binding of BH3-only proteins to the anti-apoptotic members. Furthermore, Bax is able to form oligomers and create pores in the mitochondrial outer

membrane. As a result, cytochrome C is released into the cytoplasm. Cytochrome C, apoptotic protease-activating factor 1 (Apaf-1) assemble (Cairrão & Domingos 2010). This complex recruits the inactive initiator caspase (zymogen) pro-caspase-9 and promotes trans-activation of the zymogens by the induced proximity mechanism. Afterwards, caspase-9 must stay in contact with Apaf-1 to remain fully activated and being able to execute proteolytic cleavage of the effector pro-caspases (caspase- 3, -6, -7) (Reed 2000, Elmore 2007). Then, these effector caspases are able to activate additional nucleases and together degrade apoptotic cells (Cairrão & Domingos 2010).

A second pathway underlies extrinsic activation of apoptotic signalling. When the Fas ligand binds to the Fas receptor, a signalling cascade is induced. Receptor oligomerization leads to the recruitment of the Fas-associated death domain (FADD) adaptor molecule. Via death domains initiator pro-caspases-8, and-10 (Elmore 2007, Cairrão & Domingos 2010) bind to the adaptor together forming the death-inducing signalling complex (DISC). Zymogens are again activated by the induced proximity mechanism and further cleave as well as directly activate the effector caspases. However, initiator caspases-8 and -10 are also able to link the extrinsic with the intrinsic pathway by interaction with the pro-apoptotic BH-3 only domain proteins both resulting in programmed cell death (Cairrão & Domingos 2010).

When cells are able to resist cell death resulting in uncontrolled proliferation, apoptosis depicts another hallmark of cancer (Hanahan & Weinberg 2011). The most important tumour suppressor gene is the transcription factor p53 which is mutated in about 34% of all breast cancers (Cerami et al. 2012, Gao et al. 2013, <https://www.cbioportal.org>; METABRIC, TCGA dataset; December 25.2019). Upon cellular stress such as DNA damage and hypoxia, p53 induces apoptosis via the interaction with Bcl-2 members and expression of target genes crucial for the apoptotic signalling (Lowe et al. 2004, Cairrão & Domingos 2010). Thus, when tumour suppressor p53 is inactivated due to mutations, a major key regulator in apoptosis induction is lost and cancer cells acquired resistance to cell death (Hanahan & Weinberg 2011).

1.4 Angiogenesis

Vasculature is the network that provides tissues with oxygen as well as nutrients and for its proper development a sequence of processes is needed called angiogenesis. Though, before angiogenesis may be initiated a scaffolding is established from angioblasts in the embryo during vasculogenesis (Risau 1997). This basic network made of endothelial cells named the primary capillary plexus serves for branching and sprouting of new vessels based on existing ones. This multistep procedure within the microvasculature (smallest system of the blood circuit including terminal arterioles, capillaries...) begins with destabilization of the endothelium. Its basement membrane as well as surrounding matrix is degraded and remodeled. The newly created extracellular matrix not only displays the groundwork for a new vessel but also carries growth factors. These promote proliferation and migration of endothelial cells which then lay down as a stable monolayer organized as a tube. Afterwards, mural cells (pericytes covering microvasculature or smooth muscle cells covering arteries and veins) are promoted to cover and stabilize the formed vessel (Papetti & Herman 2002, Karamysheva 2008). Finally, circulation is added to this lumen and angiogenesis is completed. Though, all these steps must be highly regulated under the influence of angiogenic mediators (Papetti & Herman 2002).

Therefore, numerous pro- and anti-angiogenic factors are crucial for the accomplishment of this procedure with some of them being implicated in tumour angiogenesis. Angiopoietin-2 (Ang2)-dependent Tie2 inhibition mediates vessel destabilization by the detachment of pericytes (Gupta & Qin 2003, Thurston & Daly 2012). Further, vascular endothelial growth factors (VEGF) are induced by hypoxia and its expression promoted by hypoxia-inducible factor (HIF). By binding to its receptor, VEGFs make the endothelial monolayer hyperpermeable for proteases and matrix components. Additionally, transforming growth factor- β (TGF- β) promotes the release of matrix metalloproteinases resulting in matrix remodeling (Papetti & Herman 2002, Gupta & Qin 2003). Together with fibroblast growth factors (FGF) as well as epidermal growth factors (EGF), VEGF stimulates proliferation in tip-cells which lead vessel growth (Papetti & Herman 2002, Gupta & Qin 2003, Karamysheva 2008). FGF plays further key roles in migration (only possible if surrounding matrix is

remodeled), and extracellular matrix organization for tube formation together with several other factors (Papetti & Herman 2002, Gupta & Qin 2003). For stabilization of the newly formed vessel mural cells are needed. Therefore, platelet-derived growth factor (PDGF) induces proliferative activity in mural cells and migration along the vessel followed by differentiation into mature pericytes (Papetti & Herman 2002). In contrast to Ang2, Ang1 leads to the activation of Tie2 by which association and vascular quiescence is maintained in endothelial cells and pericytes (Karamysheva 2008, Fukuhara et al. 2010). As a result, the expanded vasculature supplies the surrounding tissue with oxygen and nutrients. Yet, disturbances in the balance of pro- and anti-angiogenic factors can foster tumour growth (Karamysheva 2008).

Tumors can induce up- and down-regulation of angiogenic factors inducing the angiogenic switch to continuously turn on angiogenesis (Hanahan & Weinberg 2011). In various types of cancer several factors crucial for promoting the evolvment of new blood vessels such as VEGF, FGF, IL-8, and TGF- β are up-regulated in endothelial cells (Gupta & Qin 2003). Additionally, loss of Tie2 signalling in pericytes sustains tumour angiogenesis and growth (Teichert et al. 2017). All factors together foster the ability of growing malignant diseases to acquire another hallmark of cancer and thereby ensuring the supply with nutrients and oxygen during carcinogenesis (Hanahan & Weinberg 2011).

1.4.1 MicroRNAs

MicroRNAs (miRNAs) are short non-coding RNA (ncRNA) molecules with a length of 18-25 nucleotides (nt). They are found in most eukaryotes, and according to miRBase over 1,900 have been identified in human till date (<http://www.mirbase.org>; September 16.2019). These molecules are implicated in the post-transcriptional regulation by directly binding to mRNAs of protein-coding genes involved in numerous biological processes including proliferation, differentiation, growth, apoptosis and metabolic pathways. Additionally, they play a key role in various diseases governing cancer amongst others. However, before miRNAs are able to execute their inhibiting functions on target mRNAs by initiating

degradation, deadenylation or translational repression, a multistep process is essential for the generation of the mature mRNA (Khan S. et al. 2019, MacFarlane and Murphy 2010).

1.4.1.1 Biogenesis

MiRNA genes are located throughout the human genome. The majority is located in intergenic regions or inside the introns and exons of intragenic regions of protein coding and non-coding genes or untranslated and repeat sequences of the genome. MiRNAs are either organized in clusters under the control of a single promoter from a host gene leading to a polycistronic transcript which in turn is processed into the individual miRNA sequences or they are transcribed as a monocistronic transcript from their own promoter (Khan S. et al. 2019, MacFarlane and Murphy 2010).

Firstly, a miRNA gene is transcribed into the primary miRNA transcript (pri-miRNA) of more than 1 kb length by RNA polymerase II (RNA Pol II) along with various transcription factors. This pri-miRNA consists of local stem loop structures, one or more sequences for mature miRNAs, a terminal loop and single stranded RNA segments at the ends. The 5' end is modified with a 7-methyl-guanosine cap while the 3' end is polyadenylated. It is then recognized by DiGeorge syndrome critical region gene 8 (DGCR8) protein, and the endonuclease Drosha specifically cleaves the terminal single stranded RNA ends. The two proteins together are called microprocessor complex and produce the ~70 nt long precursor miRNA (pre-miRNA) with a 3' overhang. All these steps happen in the nucleus (Khan S. et al. 2019, MacFarlane and Murphy 2010).

In the next step the pre-miRNA is exported from the nucleus into the cytosol. For this, it is recognized by a transporter protein exportin 5 (EXP5). However, this protein is not only a transporter but additionally protects the RNA molecule from degradation by nucleases. Moreover, export is only possible in a Ran guanosine triphosphate (GTP)-dependent manner. The pre-miRNA/EXP5/RanGTP complex migrates through nuclear pore complexes (NPC) to the cytoplasm where RanGTP gets hydrolyzed to Ran guanosine diphosphate (GDP) by Ran

GTPase-activating protein (RanGAP). As a result, the pre-miRNA is released, RanGDP converted to RanGTP by Ran guanine nucleotide exchange factor, and further transported back into the nucleus. (Khan S. et al. 2019, MacFarlane and Murphy 2010). The released pre-miRNA is recognized by the N-terminal Piwi/Argonaute/Zwille (PAZ) domain of a multidomain enzyme called Dicer which interacts with the 3' overhang terminus of the RNA molecule. Binding occurs within the C-terminal double-strand RNA binding domain (dsRBD). Between the PAZ domain, and the RNase III domains which execute cleavage of the pre-miRNA, a platform domain is positioned. This domain generates a specific distance between the two domains to ensure that cleavage takes place exactly 21-25 nt from the 3' terminal end. This results in a ~22 nt miRNA duplex including a guide and passenger strand (Lau P. W. et al. 2012). The 5' end of the dsRNA molecule is phosphorylated and a 3' overhang is formed, both being needed for the last step of miRNA biogenesis.

RNA-induced silencing complex (RISC) assembly as the final step can be divided into loading and maturation. The 5' phosphorylation and the 3' overhang are recognized and loaded into Argonaute (Ago) proteins by their specific binding domains PAZ and middle (MID) to form the pre-RISC. The monophosphorylated 5' end is anchored to a 5' nucleotide-binding pocket positioned at the MID-PIWI interface while the PAZ domain binds the 3' end of the guide strand. Therefore, the passenger strand is more loosely bound than the guide strand. The loading is ATP-dependent and mediated by Hsc70/Hsp90 chaperone machinery as conformational changes in the Ago proteins are needed. Afterwards, the N domain of Ago plays a key role in the unwinding of the miRNA duplex and is essential for passenger strand ejection (Kwak & Tomari 2012) and formation of the mature miRISC (RISC with incorporated miRNA).

Ejection happens either slicer-dependent or slicer-independent. There are four different Ago proteins, whereas Ago2 alone exhibits endonuclease activity also known as slicer activity with its P-element Induced Wimpy testis (PIWI) domain. After the unwinding, when perfect complementary occurs, Ago2 cleaves the center of the passenger strand in a slicer-dependent manner, decreasing the stability of the duplex. In the slicer-independent ejection Ago1 and Ago3-4 use mismatches which often occur in the central regions of miRNA duplexes and slowly separate the two strands. It has to be mentioned that the 3' binding

pocket of PAZ acts as a pulling mechanism. Both slicer-dependent and slicer-independent mechanisms lead to strand separation and passenger ejection (Khan S. et al. 2019, Kwak & Tomari 2012) and result in the formation of the mature miRISC (Figure 2).

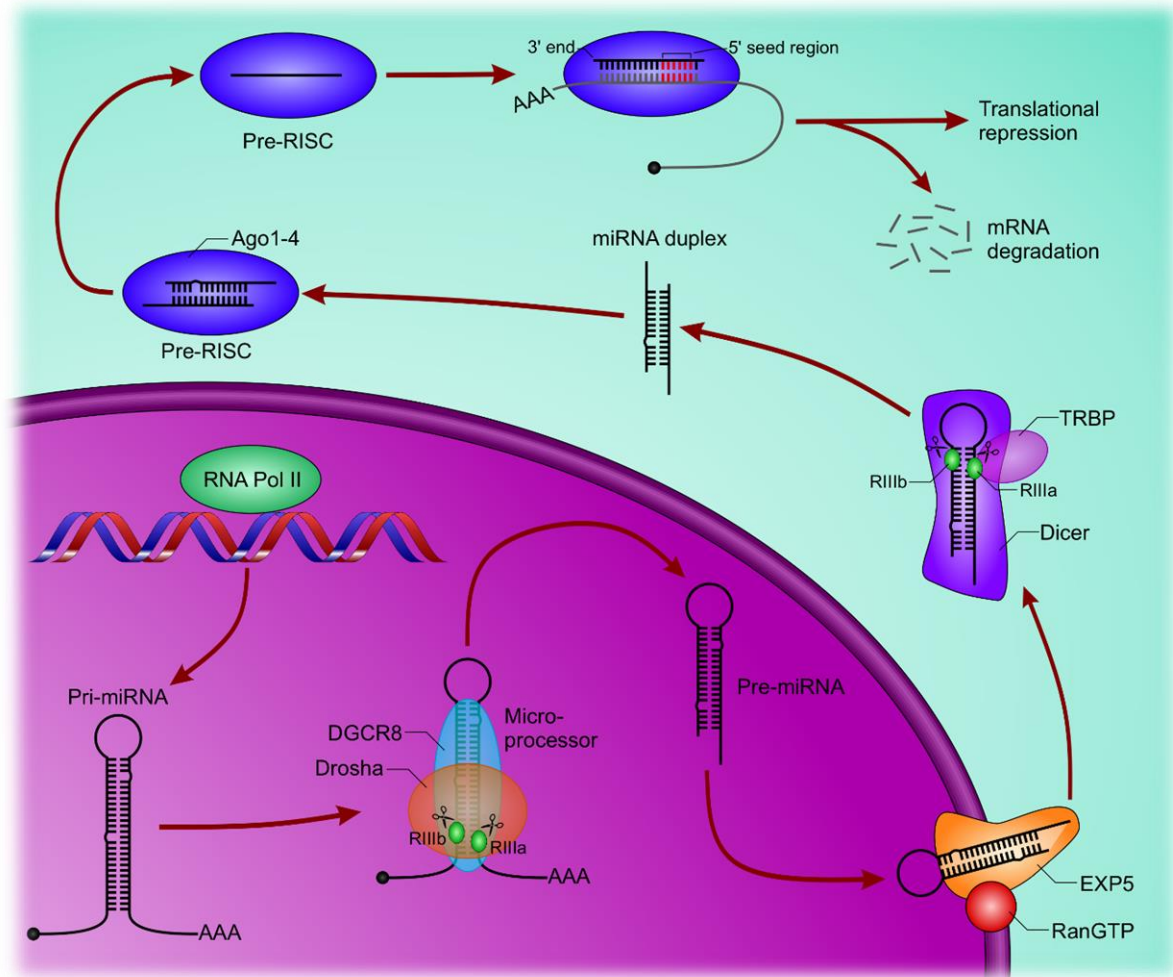


Figure 2: Illustration of miRNA biogenesis pathway. Pri-miRNA is transcribed by RNA Pol II and additional transcription factors. DGCR8 recognizes the 1 kb long molecule and Drosha specifically cleaves the capped 5' end and the polyadenylated 3' end. The newly formed pre-miRNA is then transported to the cytoplasm through EXP5/XPO5 associated with RanGTP via the nucleopore complexes. In the cytoplasm the pre-miRNA is released and the stem loop structure is removed by Dicer resulting in a ~22 nt miRNA duplex. It is further loaded into AGO1-4 where passenger strand ejection happens either slicer dependent or slicer independent and major miRISC is formed.

1.4.1.2 Gene silencing

MiRNAs exhibit their gene silencing functions on target mRNAs mainly by degradation or translational repression. In mammalian cells degradation is the most dominant method. Nt 2-7 of the 5' end represent the seed region of miRNAs which is crucial for base pairing with 3' untranslated region (UTR) of the target mRNA. Notably, the mechanism by which gene silencing is executed is determined by the grade of complementarity between the miRNA and its target mRNA (Khan S. et al. 2019, MacFarlane and Murphy 2010).

In the case of perfect complementary the mRNA is cleaved by the endonuclease activity of Ago2 and degraded by two different mechanisms. The poly-A tail is removed in the first step by decapping protein 2 (DCP2) together with other accessory proteins. Afterwards, the mRNA is degraded by cytoplasmic 5' to 3' exoribonuclease 1 (Xrn1p). Alternatively, mRNAs can be degraded by exosomes without deadenylation through their 3' to 5' exonuclease activity. Both lead to negative regulation of downstream pathways of the specific mRNAs without reversibility (Khan S. et al. 2019).

Translational repression is performed through several mechanisms before and after translational initiation. Therefore, miRISC competitively inhibits important translational factors or translation itself. mRNA bound miRISC can displace poly-A binding protein (PABP), thus prohibiting attachment of the eukaryotic translational initiation factor 4F complex (eIF4G) or it can promote dissociation of eIF4G and in turn block recruitment of ribosomal subunits. Notably, other mechanisms of translational repression need to be further investigated for example how miRISC slows down translation or terminates elongation prematurely (Khan S. et al. 2019).

1.4.1.3 MiRNAs in breast cancer

As mentioned above, miRNAs are key regulators of essential cellular processes and for that reason implicated in numerous pathologies such as cancer (Jansson & Lund 2012). While miR-10b, miR-125b, miR-145, and miR-155 are the most common aberrantly expressed miRNAs in cancer, more and more of potential oncogenic or suppressive miRNAs are

identified. MiR-132 was found to be a tumour suppressor by downregulating cell proliferation through direct binding of FOXA1 in the HER2/neu-enriched and the TNBC cell lines SKBR3 and MDA-MB-468 (Wang D. et al. 2018). Furthermore, in patients' tumorous tissues, miR-320 is downregulated and suggested to decrease proliferation, migration, and invasion (Luo L. et al. 2018). Notably, miR-1287-5p was recently found to be downregulated in breast cancer tissues and is suggested to be a possible tumour suppressor by inhibiting cell growth via the PI3K signalling pathway in TNBC cell lines (Schwarzenbacher D. et al. 2019). Due to these findings it can be said that miRNAs are an important source of manipulable regulators in breast cancer and may be potential targets for therapies.

1.5 Aim of this study

In the study of Schwarzenbacher D. et al. 2019 two miRNAs were shown to be deregulated in tissue of breast cancer patients in addition to miR-1287-5p. MiR-3150b-3p on the one hand was significantly upregulated and miR-4521 on the other hand was significantly downregulated in primary tumors compared to normal breast tissues (Schwarzenbacher D. et al. 2019). However, their role in breast carcinogenesis is not clear. Hence, the aim of my study was to comprehensively characterize the function of these two miRNAs in various breast cancer cell lines.

2 Materials

2.1 Cell culture

Table 1: Cell culture media and ingredients

Product name	Company	Headquarters
HyClone Ham's Nutrient Mixture F-12 with 1 mmol/l L-glutamine	GE Heath Care Life Sciences	Chicago, Illinois, USA
DMEM high glucose with 4.5 g/l D-glucose and L-glutamine	Thermo Fisher Scientific	Waltham, Massachusetts, USA
RPMI Medium 1640 with L-glutamine	Thermo Fisher Scientific	Waltham, Massachusetts, USA
EMEM with L-glutamine	Lonza	Basel, Switzerland
EBM-2 Basal medium	Lonza	Basel, Switzerland
EGM-2 MV SingleQuots Supplement pack	Lonza	Basel, Switzerland
Fetal bovine serum (FBS) superior	Biochrom	Berlin, Germany
Penicillin/Streptomycin	Thermo Fisher Scientific	Waltham, Massachusetts, USA
HEPES (1 mol/l)	Thermo Fisher Scientific	Waltham, Massachusetts, USA
Hydrocortisone	Merck	Darmstadt, Germany
Insulin solution from bovine pancreas (10 mg/ml)	Merck	Darmstadt, Germany
L-glutamine (200 mM)	Biochrom	Berlin, Germany
Sodium pyruvate (100 mM)	GE Heath Care Life Sciences	Chicago, Illinois, USA
Phosphate buffered saline (PBS), pH 7.4 (1x), without CaCl ₂ , MgCl ₂	Thermo Fisher Scientific	Waltham, Massachusetts, USA
2.5 % Trypsin (10X)	Thermo Fisher Scientific	Waltham, Massachusetts, USA

Trypan Blue	Biorad	Hercules, California, USA
-------------	--------	---------------------------

2.2 Transfection

2.2.1 Reagents

Table 2: Transfection reagents

Product name	Company	Headquarters
HiPerFect transfection reagent	Qiagen	Hilden, Germany
RNase-free water	Qiagen	Hilden, Germany

2.2.2 MiRNA mimics and inhibitors

Table 3: Mimic and inhibitor sequences

Product group	Company	Headquarters
miRCURY LNA miRNA mimic (5)	Qiagen	Hilden, Germany
Product name	Sequence 5'-3'	
Negative control miRCURY LNA M	UCACCGGGUGUAAAUCAGCUUG	
hsa-miR-3150b-3p	UGAGGAGAUCGUCGAGGUUGG	
hsa-miR-4521	GCUAAGGAAGUCCUGUGCUCAG	
Product group	Company	Headquarters
miRCURY LNA miRNA inhibitor (5)	Qiagen	Hilden, Germany
Product name	Sequence 5'-3'	
Negative control A	TAACACGTCTATACGCCCA	
hsa-miR-3150b-3p	CAACCTCGACGATCTCCTCA	
hsa-miR-4521	TGAGCACAGGACTTCCTTAG	

2.3 RNA purification

Table 4: Reagents for RNA purification

Product name	Company	Headquarters
Qiazol Lysis Reagent	Qiagen	Hilden, Germany
1-bromo-3-chloropropane (BCP)	Merck	Darmstadt, Germany
Isopropanol/2-propanol for analysis	Merck	Darmstadt, Germany
Ethanol absolut for analysis	Merck	Darmstadt, Germany
Milli-Q water	Merck	Darmstadt, Germany
RNase-free water	Qiagen	Hilden, Germany

2.4 cDNA synthesis

Table 5: Reagents for cDNA synthesis

Product name	Company	Headquarters
miScript II RT Kit	Qiagen	Hilden, Germany
Contents		
5x miScript HiFlex buffer		
10x miScript nucleics mix		
RNase-free water		
miScript reverse transcriptase mix		

2.5 Real-time qPCR

2.5.1 Kit

Table 6: Reagents for real-time qPCR

Product name	Company	Headquarters
miScript SYBR Green PCR Kit	Qiagen	Hilden, Germany
Contents		
2x QuantiTect SYBR Green PCR master mix		
10x miScript Universal primer		
10x miScript Primer assay		
RNase-free water		

2.5.2 Primer

Table 7: Primer sequences

Product group	Company	Headquarters
10x miScript primer assays	Qiagen	Hilden, Germany
Product name	Sequence 5'-3'	
Negative control miRCURY LNA M	UCACCGGGUGUAAAUCAGCUUG	
hsa-miR-3150b-3p	UGAGGAGAUCGUCGAGGUUGG	
hsa-miR-4521	GCUAAGGAAGUCCUGUGCUCAG	

2.6 WST-1 metabolic proliferation assay

Table 8: Reagents for proliferation assay

Product name	Company	Headquarters
Cell proliferation reagent WST-1	Roche	Basel, Switzerland

2.7 Colony forming unit assay

Table 9: Reagents for colony forming unit assay

Product name	Company	Headquarters
Methanol $\geq 99\%$, for synthesis	Roth	Karlsruhe, Germany
Acetic acid (glacial) 100%	Merck	Darmstadt, Germany
Crystal violet, ACS reagent, $\geq 90\%$ anhydrous basis	Merck	Darmstadt, Germany
Milli-Q water	Merck	Darmstadt, Germany
PBS, pH 7.4 (1x), without CaCl ₂ , MgCl ₂	Thermo Fisher Scientific	Waltham, Massachusetts, USA

2.8 Cell cycle analysis

Table 10: Reagents for cell cycle analysis

Product name	Company	Headquarters
PBS, pH 7.4 (1x), without CaCl ₂ , MgCl ₂	Thermo Fisher Scientific	Waltham, Massachusetts, USA
Fetal bovine serum superior	Biochrom	Berlin, Germany

Ethanol absolut for analysis	Merck	Darmstadt, Germany
Sodium citrate tribasic dihydrate, ≥98%	Merck	Darmstadt, Germany
Triton® X-100	Merck	Darmstadt, Germany
RNase A, DNase and Protease-free	Thermo Fisher Scientific	Waltham, Massachusetts, USA
Propidium iodide (PI), 1.0 mg/ml	Merck	Darmstadt, Germany
Milli-Q water	Merck	Darmstadt, Germany

2.9 Apoptosis assay

Table 11: Reagents for Caspase-Glo® 3/7 assay

Product name	Company	Headquarters
Caspase-Glo® 3/7 assay	Promega	Madison, Wisconsin, USA
Contents		
Caspase-Glo® 3/7 buffer		
Caspase-Glo® 3/7 substrate		

2.10 *In vitro* angiogenesis assay

Table 12: Reagents for angiogenesis assay

Product name	Company	Headquarters
ECMatrix Gel solution	Merck	Darmstadt, Germany
ECMatrix Diluent buffer, 10x	Merck	Darmstadt, Germany
Calcein, AM (4 mM)	Thermo Fisher Scientific	Waltham, Massachusetts, USA

3 Equipment

Table 13: Equipment

Name	Company	Headquarters
Biofuge fresco	Heraeus	Hanau, Germany
Cell counting slides	Biorad	Hercules, California, USA
Centrifuge FVL-2400N Combi-Spin	Biosan	Riga, Latvia
CytoFlex S flow cytometer	Beckmann Coulter	Brea, California, USA
Heating table	Medax	Neumünster, Germany
Incubator Heracell 240 CO2	Heraeus	Hanau, Germany
IX51 Inverted microscope	Olympus	Tokio, Japan
LightCycler 480 System	Roche	Basel, Switzerland
LUMIstar	SMG Labtech	Kansas City, Missouri, USA
Multifuge 1L-R	Heraeus	Hanau, Germany
MyCycler thermal cycler	Biorad	Hercules, California, USA
NanoDrop 2000c Spectrophotometer	Thermo Fisher Scientific	Waltham, Massachusetts, USA
Pipette Controller accu-jet pro	Brand	Wertheim am Main, Germany
Repeater pipette	Eppendorf	Hamburg, Germany
Shaker DRS-12	ELMI	Calabasas, California, USA
SPECTROstar Omega	SMG Labtech	Kansas City, Missouri, USA
TC20 automated cell counter	Biorad	Hercules, California, USA
TH4-200 Power supply	Olympus	Tokio, Japan
U-RFL-T Power supply	Olympus	Tokio, Japan
Water bath Unitronic OR	P Selecta	Abrera, Barcelona
Xplorer plus, 8-channel pipette	Eppendorf	Hamburg, Germany

4 Methods

4.1 *In silico* analysis

4.1.1 Overall survival analysis

The Kaplan-Meier (KM) plotter (<https://kmplot.com>) was used to analyze overall survival (OS) for miR-3150b-3p and miR-4521 in breast cancer. Using the TCGA dataset, KM plot curves including all breast cancer patients (n=1061) and plots including only TNBC patients (n=97) were created. The patients were split into high and low expression of the distinct miRNA by using an algorithm of auto select function. For miR-3150b-3p the follow-up threshold was set to 60 months and for miR-4521 to 120 months.

4.1.2 Housekeeping gene analysis

To determine the stability of housekeeping genes the algorithm geNorm was used. Five candidates (RNU6B, SNORD61, SNORD68, SNORD72, and SNORD95) were used as internal controls in 11 different cell lines in real-time qPCR. The Δ ct-values were then imported to the geNorm excel file. Furthermore, an algorithm calculates a gene expression normalization factor based on the geometric mean of the housekeeper and further gene stability value (M). A low M value indicates a stable reference gene (i.e. the lowest variation of the same gene between different samples) compared to other candidates (Hellemans et al. 2007).

4.2 Cell culture

The luminal A MCF7 and T-47D, the luminal B BT-474, the HER2/neu positive SKBR3 and HCC1419, the TNBC cell lines HCC1937, MDA-MB-468, BT-549, MDA-MB-231, and SUM159 as well as the non-tumorous MCF-12A and HUVEC were used in this master's thesis. MCF7 were cultured in EMEM with L-glutamine containing 10% FBS, 1% penicillin/streptomycin (for all used cell lines: penicillin: 10,000 units/ml, streptomycin: 10,000 μ g/ml), and 1% sodium pyruvate, T-47D in RPMI medium 1640 with L-glutamine containing 10% FBS and 1% penicillin/streptomycin, BT-474 in RPMI medium 1640 with L-glutamine containing 20% FBS, 1% penicillin/streptomycin, 2 mM L-glutamine and 10 μ g/ml insulin, SKBR3, HCC1419, HCC1937 and BT549 in RPMI medium 1640 with L-glutamine containing 10% FBS and 1%

penicillin/streptomycin, MDA-MB-231 and MDA-MB-468 in DMEM high glucose with 4.5 g/l D-glucose and L-glutamine containing 10% FBS and 1% penicillin/ streptomycin, SUM159 in HyClone Ham's nutrient mixture F-12 with 1 mmol/l L-glutamine containing 5% FBS, 1% penicillin/streptomycin, 10 mmol/l HEPES, 1 µg/ml hydrocortisone and 5 µg/ml insulin, MCF-12A in DMEM high glucose with 4.5 g/l D-glucose/Ham's F-12 with 1 mmol/l L-glutamine 1:1 containing 5% horse serum, 1% penicillin/streptomycin, 20 ng/ml human EGF, 100 ng/ml cholera toxin, 0.01 mg/ml bovine serum and 500 ng/ml hydrocortisone, and HUVEC in EBM-2 basal medium containing the EGM-2 MV SingleQuots Supplement pack. Sub culturing was performed one to two times a week and for this 0.25% trypsin in PBS was used. Therefore, cells were incubated with this solution for 5 min at 37°C for detachment. Afterwards, the trypsin was neutralized with complete growth medium.

4.3 Fast-forward transfection

After detachment of cells as in 4.2 cell number was determined. First cells were collected in 15 ml tubes and centrifuged at 800 rpm. The pellet was further dissolved in 10 ml of complete growth medium. In the next step the cell number was determined. For this, 10 µl cell suspension were mixed with 10 µl trypan blue. 10 µl of this mix were transferred onto cell counting slides and the cell number was measured with the TC20 automated cell counter. Afterwards, transfection mix was prepared for transfection in 6-well plates according to Table 14.

Table 14: Transfection mix

Component	Volume/reaction
Mimics or inhibitors (20 µM)	3 µl
Serum-free medium	87 µl
HiPerFect transfection reagent	10 µl

MiRNA mimics were diluted in serum-free medium so they reach a concentration of 10 nM in a final volume of 3 ml. For miRNA inhibitors a final concentration of 50 nM was used. 10 µl HiPerfect transfection reagent were added last. The transfection mix was mixed by short

vortexing and incubated at room temperature for approximately 15 min to allow the formation of transfection complexes. In the meantime, the cell suspension was diluted with complete growth medium to a seeding density so cells would reach confluence after 48 hours of incubation in a 6-well plate. 2.9 ml of the diluted cell suspension were transferred into each well, respectively. Subsequently, 100 μ l of the transfection mix were added drop-wise to the cells and the plate was rocked back and forth several times to disperse the cells and especially the transfection mix equally and quickly in the well as mimics and inhibitors are toxic in high concentrations. Finally, the cells were incubated with the transfection complexes under their normal growth conditions for 48 hours.

4.4 Reverse transfection

Cell detachment and cell counting was executed as in 4.3. The transfection mix was prepared according to Table 15.

Table 15: Transfection mix

Component	Volume/reaction
Mimics or inhibitors (20 μ M)	0.1 μ l
Serum-free medium	24.15 μ l
HiPerFect transfection reagent	0.75 μ l

MiRNA mimics were diluted in serum-free medium so they reach a concentration of 10 nM in a final volume of 200 μ l. For miRNA inhibitors a final concentration of 50 nM was used. 0.75 μ l HiPerfect transfection reagent were added last. The transfection mix was mixed by short vortexing and incubated at room temperature for approximately 15 min to allow the formation of transfection complexes. In the meantime, the cell suspension was diluted with medium to a seeding density so cells would not reach confluence after 120 hours of incubation in a 96-well plate. 25 μ l of the transfection mix were transferred into each well, respectively. Subsequently, 175 μ l of the cell suspension were added to each well. Finally, the cells were incubated with the transfection complexes under their normal growth conditions for 24-120 hours.

4.5 Purification of total RNA

After cells were washed with PBS, Qiazol lysis reagent was used for harvesting the RNA. For a T-75 flask 3-4 ml of Qiazol reagent was added to the cells and the lysate transferred into 1.5 ml Eppendorf tubes in 1 ml aliquots. For a six-well plate 1 ml Qiazol was used for each well. Afterwards, the cells were passed through a needle (0.7 x 50 mm) 5 times to disrupt cell membranes followed by 15 min of incubation at room temperature to dissociate

nucleoprotein complexes. In the meantime, 75% ethanol was prepared by adding 12.5 ml ethanol absolute to 37.5 ml Milli-Q water and cooled down to -20°C. After the incubation 0.1 ml 1-bromo-3-chloropropane was added to the lysate and the mixture was shaken vigorously for 15 sec followed by 3 min of incubation at room temperature. The samples were then centrifuged at 13,000 g and 4°C for 15 min. Meanwhile, 0.5 ml isopropanol were prepared in fresh 1.5 ml Eppendorf tubes. After the centrifugation a clear phase-separation should occur with RNA in the upper aqueous, DNA in the interphase and proteins in the lower organic phase. The upper phase was transferred carefully to the tube with the prepared isopropanol and the mixture shaken vigorously for 15 sec. The samples were centrifuged at 13,000 g and 4°C for 30 min. Afterwards, the pellet was formed on the bottom of the tube and from this step on the sample was always put on ice. The supernatant was discarded and the pellet washed with 1 ml cold 75% ethanol followed by centrifugation at 13,000 g and 4°C for 5 min. The washing steps were repeated three times. After final centrifugation, the whole supernatant was removed carefully and the pellet dried at room temperature until it got translucent. Dependent on the size of the pellet 15-25 µl pre-warmed nuclease-free water (40°C) were added to each pellet and dissolved at 40°C for 10 min.

The concentration of the isolated RNA was determined by measuring the absorbance at 260 nm. The absorbance ratio 260/280 nm was used to assess the purity of nucleic acids and should be approximately 2.0 for RNA.

4.6 CDNA synthesis

CDNA synthesis was performed by reverse transcription with the miScript II RT Kit. For this, template RNA was thawed on ice, and 10x miScript nucleics mix and 5x miScript HiFlex buffer were thawed at room temperature. When using the miScript HiFlex buffer mature miRNAs, precursor miRNAs, noncoding RNAs and mRNAs are converted into cDNA. Each solution was mixed followed by a short centrifugation to collect the residual liquid from the sides of the tubes and then stored on ice. Afterwards, the reverse transcription master mix was prepared on ice according to Table 16.

Table 16: RT master mix

Component	Volume/reaction
5x miScript HiFlex buffer	4 μ l
10x miScript nucleics mix	2 μ l
miScript reverse transcriptase (RT) mix	2 μ l
RNase-free water	variable
template RNA	variable

8 μ l of the master mix were added to each tube of a 0.2 ml PCR soft strip. 1 μ g template RNA was added separately and filled up with RNase-free water to a final volume of 20 μ l. The reaction mix was mixed gently and centrifuged briefly followed by incubation in the thermal cycler. First the solution was incubated at 37°C for 60 min followed by incubation at 95°C for 5 min to inactivate the RT. After the program was finished, the cDNA was stored undiluted at -20°C or immediately diluted for quantification with real-time qPCR.

4.7 Real-time qPCR

Quantification with real-time qPCR was performed using the miScript SYBR Green PCR Kit. 2x QuantiTect SYBR Green PCR master mix, which includes the HotStarTaq DNA polymerase to avoid unspecific priming prior to the start of the PCR, 10x miScript Universal primer, 10x miScript Primer assay, RNase-free water and cDNA were thawed at room temperature. The cDNA was diluted to reach a final concentration of 1 ng for the detection of miRNAs in the reaction mix.

Table 17: PCR master mix

Component	Volume/reaction (96-well)	Volume/reaction (384-well)
2x QuantiTect SYBR Green PCR master mix	12.5 μ l	5 μ l
10x miScript universal primer	2.5 μ l	0.4 μ l
10x miScript primer assay	2.5 μ l	0.4 μ l
RNase-free water	5.5 μ l	3.2 μ l
template cDNA (0.5 ng/ μ l / 1 ng/ μ l)	2 μ l	1 μ l

The master mix was prepared according to Table 17, mixed by pipetting it up and down and 23 μ l were provided in each well of a 96-well plate. Afterwards, 2 μ l diluted cDNA were added to each well, respectively. For a 384-well plate the whole reaction mix was prepared in soft strips and added to the wells with a multi-channel pipette. This mix was mixed thoroughly by shaking followed by short centrifugation. Afterwards, 10 μ l reaction mix were added to each well, respectively. The plates were sealed with optical adhesive sealing foil and centrifuged at 900 rpm for 30 sec to collect all residual liquid from the sides. The cycle program was chosen according to Table 18. The initial activation was needed because a hot-start polymerase was used.

Table 18: Cycle program

Step	Time	Temperature
Initial activation	15 min	95°C
3-step cycling for 40 cycles:		
Denaturation	15 s	94°C
Annealing	30 s	55°C
Elongation	30 s	70°C

4.8 WST-1 metabolic proliferation assay

Cells were seeded and transfected as in 4.4. For each time point (24-120 hours) cells were seeded in separate 96-well plates. After 24, 48, 72, 96, and 120 hours 100 μ medium were removed from each well, and 10 μ l/well WST-1 reagent added. Cells were then incubated under their normal growth conditions for 180 min. During this time, tetrazolium salts of the proliferation reagent are converted by the mitochondrial succinate-tetrazolium-reductase system to formazan. This results in a color change. The absorbance, reflecting the amount of living cells in a well, was measured at 450 nm as well as 620 nm as reference at every time point (24 h, 48 h, 72 h, 96 h, and 120 hours) after 30-180 min after addition of the WST-1 reagent to the cells.

4.9 Colony forming unit assay

Cell detachment, cell counting, and transfection was executed as in 4.3. After 48 hours of incubation cells were harvested with 0.5 ml of 0.25% trypsin in PBS, cell number determined again as before and the cells seeded in a very low density. Therefore, it is ensured that colonies rise from one single cell. After the formation of countable colonies, they were stained with crystal violet. For this, a fixing and a staining solution was prepared. Methanol and acetic acid was mixed 4:1 for the fixing solution. In order to prepare the staining solution 0.25 mg crystal violet powder were dissolved in 40 ml Milli-Q water and 10 ml methanol. For the staining, cells were washed two times with 2 ml of PBS and removed it afterwards. 1 ml of the fixing solution was added to each well, respectively, and incubated at room temperature for 10 minutes. The fixing solution was removed completely and the 6-well plate dried for about 30 min. For the staining, 1 ml of the staining solution was added to each well and incubated at room temperature under agitation for 10 min. The solution was removed and the colonies were washed three times with Milli-Q water. Furthermore, the water was removed and the plate dried overnight. Finally, the colonies were counted manually.

4.10 Cell cycle analysis

Transfection was executed as in 4.3. However, 25 mm² flasks were used and a final volume of 5 ml. After 48 h of incubation with the transfection mix, cells were detached with 0.25% trypsin in PBS followed by centrifugation at 200 g and 4°C for 4 min. The pellet was resuspended and centrifugation was repeated. Afterwards, the pellet was resuspended in 5 ml PBS and the cell number determined. About 700,000 cells were again centrifuged at 200 g and 4°C for 4 min and further dissolved in 500 µl PBS. 5 ml pre-cooled 70% ethanol were added to the cells under vortexing for fixation and stored at 4°C for up to two weeks. Afterwards, the staining solution (PI-hypotonic lysis buffer) was prepared according to Table 19.

Table 19: PI-hypotonic lysis buffer

Component	Volume/reaction
0.1 % Sodium citrate	100 µl
10 % Triton® X-100	100 µl
RNase A (10 mg/ml)	100 µl
PI (1 mg/ml)	500 µl
Milli-Q water	9.2 ml

The fixed cells were centrifuged at 1000 g for 4 min followed by two washing steps with 5 ml 0.5% FBS in PBS. After another centrifugation step the pellet was resuspended in 200 µl PI-hypotonic lysis buffer followed by 20 min of incubation at room temperature. Samples were put on ice and analyzed via fluorescence-activated cell sorting (FACS).

4.11 Apoptosis assay

First, the substrate was diluted in 10 ml buffer. Cells were seeded and transfected as in 4.4. For each time point (48-72 hours) cells were seeded in separate 96-well plates. After 48 and 72 hours medium was removed from each well, and 100 μ l/well Caspase-Glo[®] 3/7 reagent added. Cells were incubated in the dark at room temperature for 30 min. During this time, activated effector caspases react with the apoptosis reagent. This results in fluorescence, which can be quantified. Afterwards, the cell lysates were transferred into a white 96-well plate. The emission was measured at 450 nm at every time point (48 h and 72 hours) after 90 min after addition of the Caspase-Glo[®] 3/7 reagent to the cells.

4.12 *In vitro* angiogenesis assay

Procedure was executed as in 4.9. Before harvested transfected cells were seeded the matrix was prepared in a 96-well plate. The ECMatrix Gel solution was thawed overnight at 4°C. Additionally, pipette tips, multiwell plates, and tubes were pre-cool also at 4°C. On the day of the seeding the ECMatrix Diluent buffer was thawed on ice and then 100 μ l added to 900 μ l of the gel solution followed by careful mixing without creating air bubbles. 50 μ l of this solution were transferred to each well of the pre-cooled 96-well plate followed by incubation at 37°C for at least one hour to allow the matrix to solidify. During this time the cell suspension was prepared with an appropriate cell number for tubes to form. 150 μ l cell suspension were added to each well and incubated for 16 hours under their normal growth conditions. Afterwards, 4 μ l calcein, AM were added to each well for a final concentration of 2 μ g/ml to stain living cells. Tubes were imaged after 1 hour of additional incubation and analyzed with ImageJ.

5 Results

5.1 *In silico* analysis

5.1.1 Overall survival regarding expression of miR-3150b-3p and miR-4521

For both miRNAs OS curves were generated with data for all breast cancer subtypes and triple negative in specific to assess their clinical relevance. The follow-up threshold was set

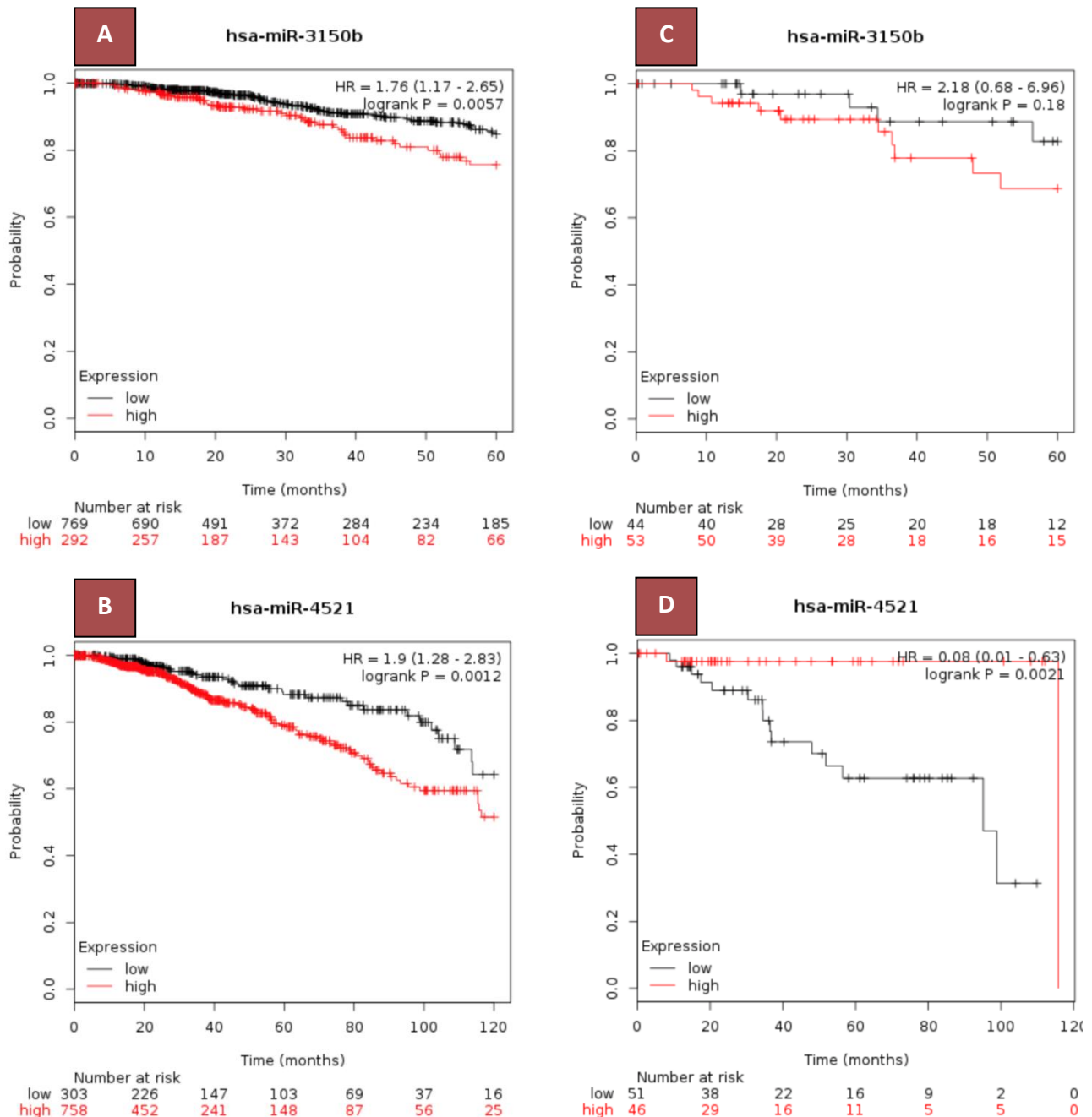


Figure 3: OS curves for miR-3150b-3p and miR-4521 in breast cancer. In the online tool KM-Plotter OS curves were generated for both miRNAs in all breast cancer subtypes (A-B) and TNBC (C-D) in specific. Higher expression levels of (A-B) miR-3150b-3p led to a shorter OS in all breast cancer subtypes and TNBC. (C-D) MiR-4521 led to a worse outcome when highly expressed only in all subtypes while a low expression resulted in shorter OS in TNBC. Hazard ratio with 95 % confidence intervals and logrank P value was calculated.

to 60 months for miR-3150b-3p and 120 months for miR-4521 as there were significant differences between the two groups.

MiR-3150b-3p showed a significantly higher survival probability when expressed at lower levels after 60 months ($p=0.0057$) in all breast cancer subtypes but no significance was obtained when focusing only on TNBC ($p=0.18$). In the case of miR-4521 a significantly higher survival probability was observed in all breast cancer subtypes ($p=0.0012$) and in TNBC ($p=0.0021$) when expressed at a lower level.

5.1.2 Determination of a stable housekeeping gene

For each of the candidate housekeeping genes an M value was obtained (RNU6B=0.07, SNORD61=0.057, SNORD68=0.066, SNORD72=0.08, SNORD95=0.051). RNU6B and SNORD72 showed the highest variation across all used cell lines (KPL-1, MCF-7, T-47D, BT-474, SKBR3, HCC1937, MDA-MB-468, BT-549, MDA-MB-231, SUM159, and HCC1914), while SNORD61 and SNORD95 were most stably expressed.

5.2 Expression analysis of miRNAs in different breast cancer cell lines

To investigate gene expression of miR-3150b-3p and miR-4521 in breast cancer cell lines, qRT-PCR was performed with isolated total RNA from eleven different breast cancer cell lines. Therefore, MCF-7, T-47D, BT-474, HCC1419, SKBR3, HCC1937, MDA-MB-468, BT-549, MDA-MB-231, SUM159, and MCF-12A were grown under their normal conditions and total RNA was purified from cells in three different passages. Hence, the expression analysis was conducted in three independent biological replicates (n=3). SNORD61 and SNORD95 were used as housekeeping genes and MCF-12A as control, which is an immortalized non-cancerous breast cell line.

Figure 4 shows that the expression levels of miR-3150b-3p varied from slightly decreased to slightly increased in most cell lines in comparison with the MCF-12A cell line. Only the HCC1419 cell line had significantly increased miR-3150b-3p expression levels whereas miR-4521 was significantly increased in MDA-MB-231 compared to the control. Both miRNAs displayed a trend to be up-regulated in the TNBC cell lines MDA-MB-231 and SUM159, and miR-4521 was additionally up-regulated, in BT-549. The TNBC cell lines BT-549, MDA-MB-231, and SUM159 were used for downstream assays.

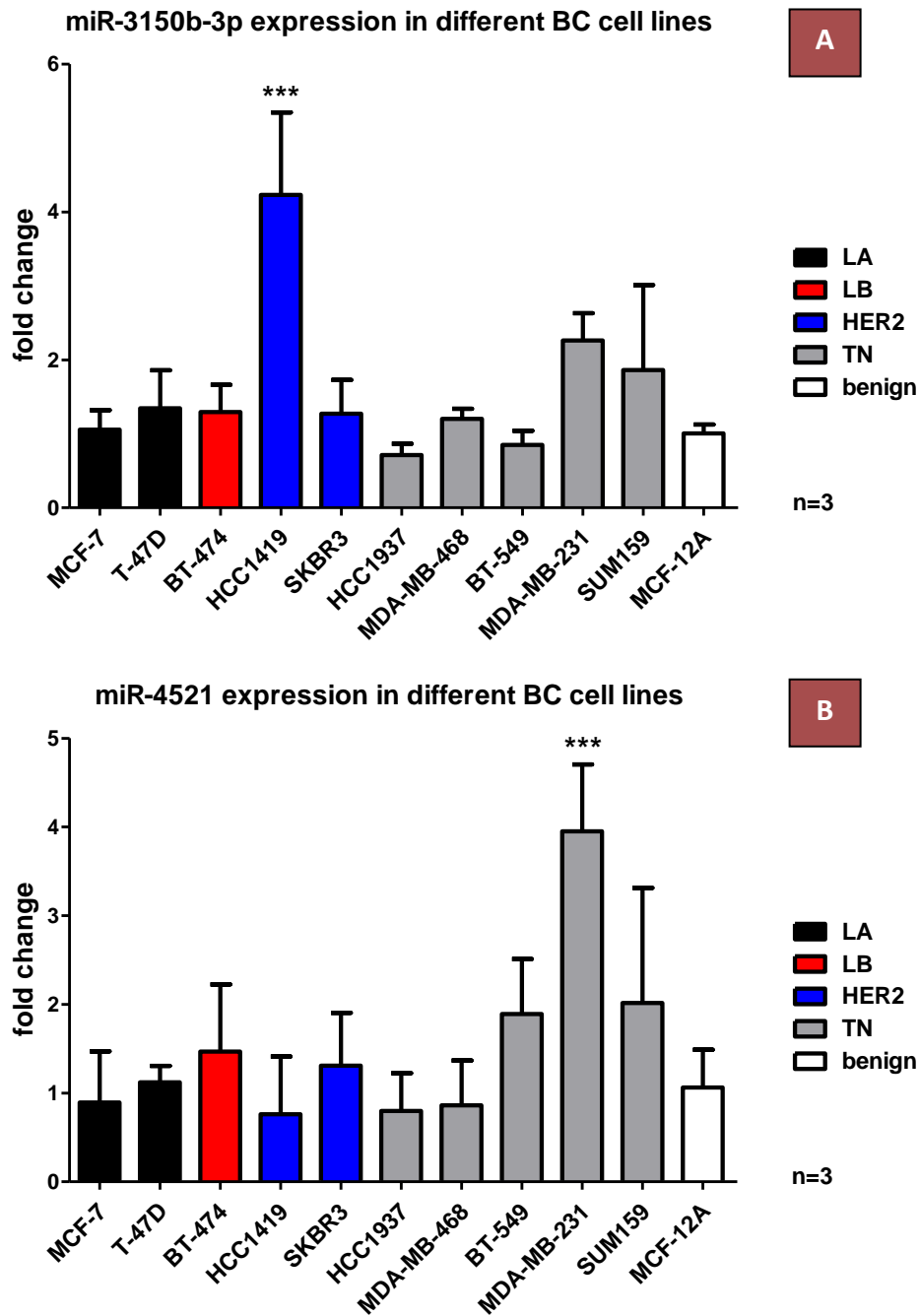


Figure 4: miR-3150b-3p and miR-4521 expression in different breast cancer cell lines. Breast cancer cell lines and the immortalized control cell line MCF-12A were harvested in three different passages and the expression of (A) miR-3150b-3p and (B) miR-4521 were analyzed by real-time qPCR. MiR-3150b-3p was only significantly up-regulated in HCC1914 while miR-4521 was significantly up-regulated in MDA-MB-231 and slightly higher expressed in BT-549 and SUM159. Data are shown as mean with standard deviation. Significance was determined by one-way ANOVA with Dunnett post-test ($p < 0.05 = *$, $0.01 = **$, $0.001 = ***$). LA=luminal A, LB=luminal B, HER2=HER2-enriched, TN=triple negative, BC=breast cancer.

5.3 Manipulation of miRNA expression levels using mimics and inhibitors

To achieve an overexpression or a knock-down of miR-3150b-3p and miR-4521, BT-549 (Figure 5), SUM159 (Figure 6), and the endothelial cell line HUVEC (Figure 7) were transfected with mimics and inhibitors for both miRNAs. The total RNA was purified after 48 h of transfection. Afterwards, the RNAs concentration and purity was measured and used for cDNA synthesis. Furthermore, real-time qPCR was performed to analyze transfection efficiency.

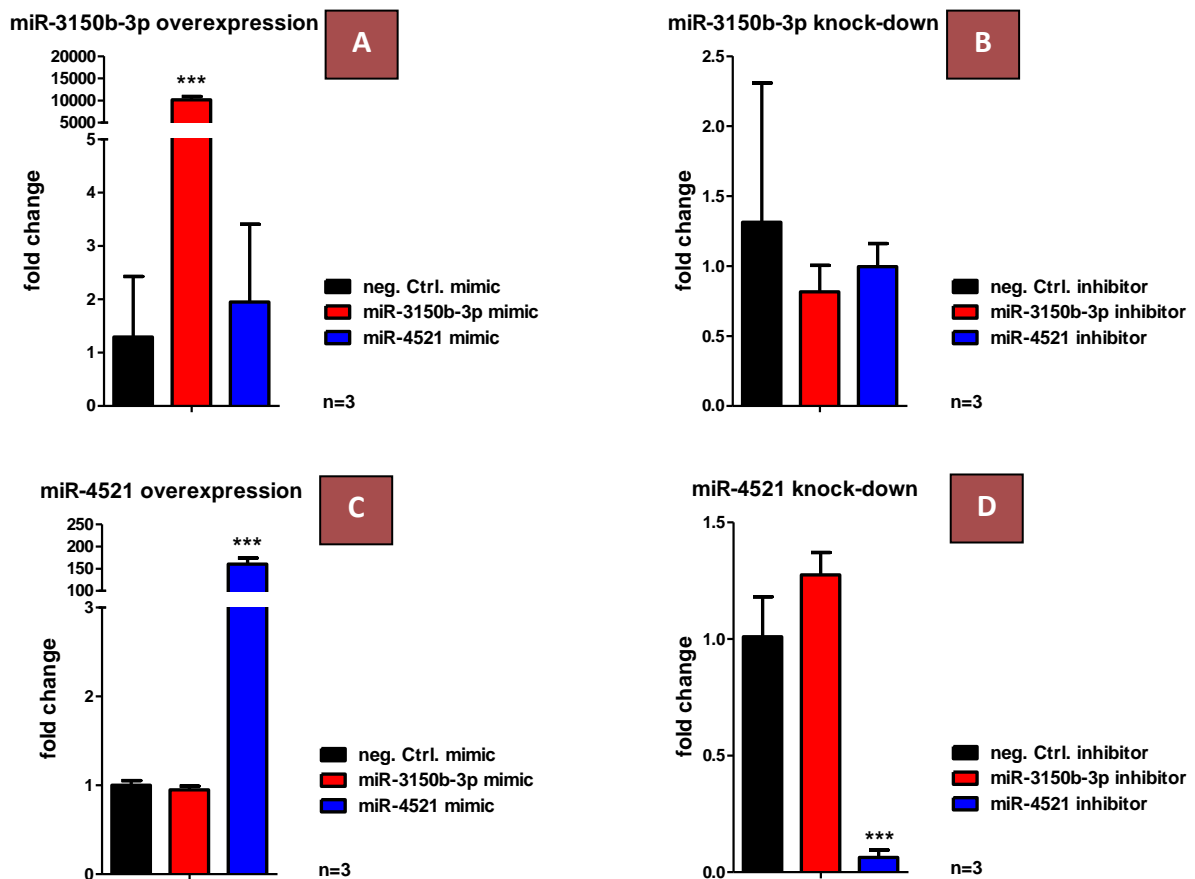


Figure 5: Transfection efficiency of mimics and inhibitors in BT-549. BT-549 were transfected with (A-B) miR-3150b-3p and (C-D) miR-4521 (A and C) mimics and (B and D) inhibitors to further analyze the efficiency of transfection with real-time qPCR. Both miRNAs were significantly overexpressed while only miR-4521 was successfully knocked down. Significance was determined by one-way ANOVA with Dunnett post-test ($p \leq 0.05 = *$, $0.01 = **$, $0.001 = ***$).

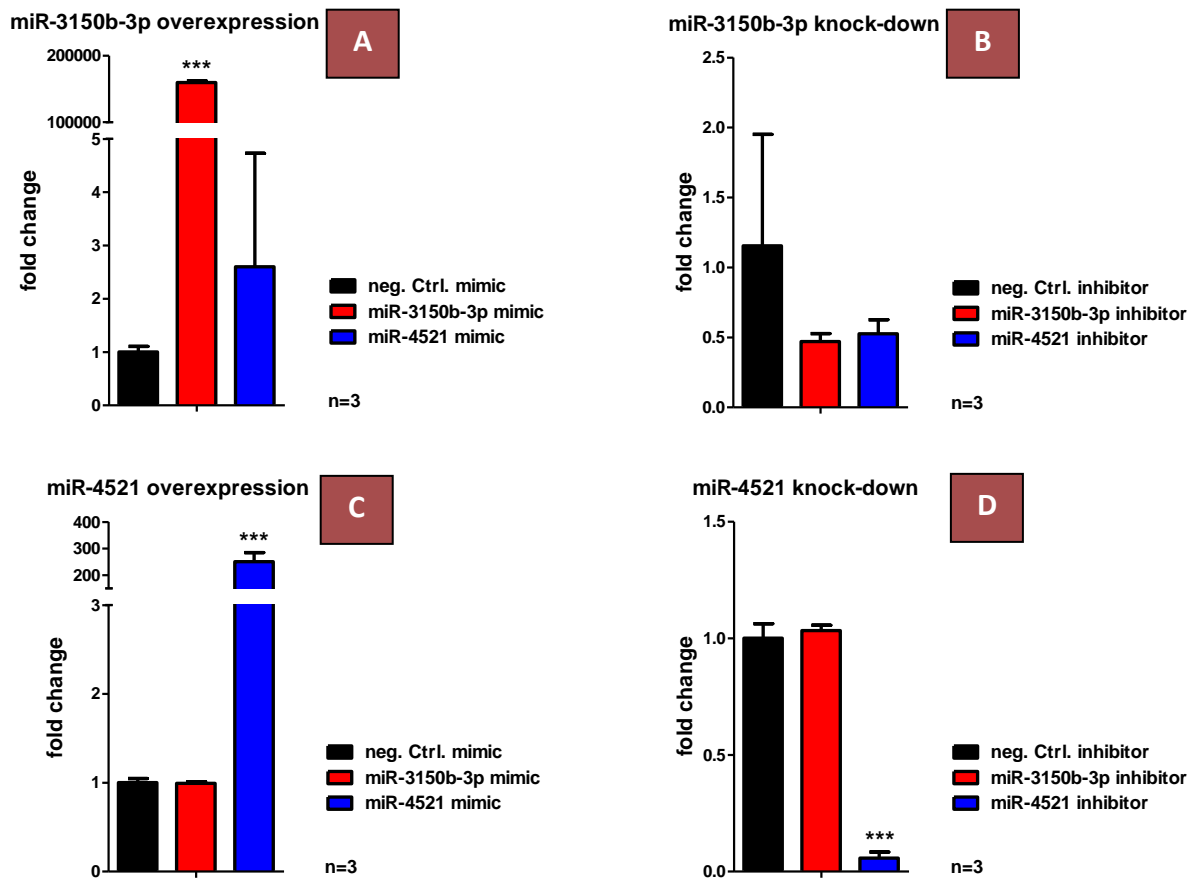


Figure 6: Transfection efficiency of mimics and inhibitors in SUM159. SUM159 were transfected with (A-B) miR-3150b-3p and (C-D) miR-4521 (A and C) mimics and (B and D) inhibitors to further analyze the efficiency of transfection with real-time qPCR. Both miRNAs were significantly overexpressed while only miR-4521 was successfully knocked down. Significance was determined by one-way ANOVA with Dunnett post-test ($p \leq 0.05 = *$, $0.01 = **$, $0.001 = ***$).

A concentration of 10 nM for the mimics was sufficient to achieve a significant increase in both miRNAs. Inhibitors were used in a concentration of 50 nM. Taking into account, that miR-3150b-3p was already expressed at a very low level in all cell lines, only a slight knock-down was obtained. Additionally, it can be observed that miR-3150b-3p is slightly modulated by miR-4521 mimic and inhibitor. The transfection with miR-4521 inhibitors led to almost a complete knock-down. The same effects were observed in all three cell lines but with different efficiencies. The expression levels of the miRNAs could not be statistically evaluated in HUVEC as only one replicate was analyzed. The same concentrations for the mimics and inhibitors were used for all downstream assays.

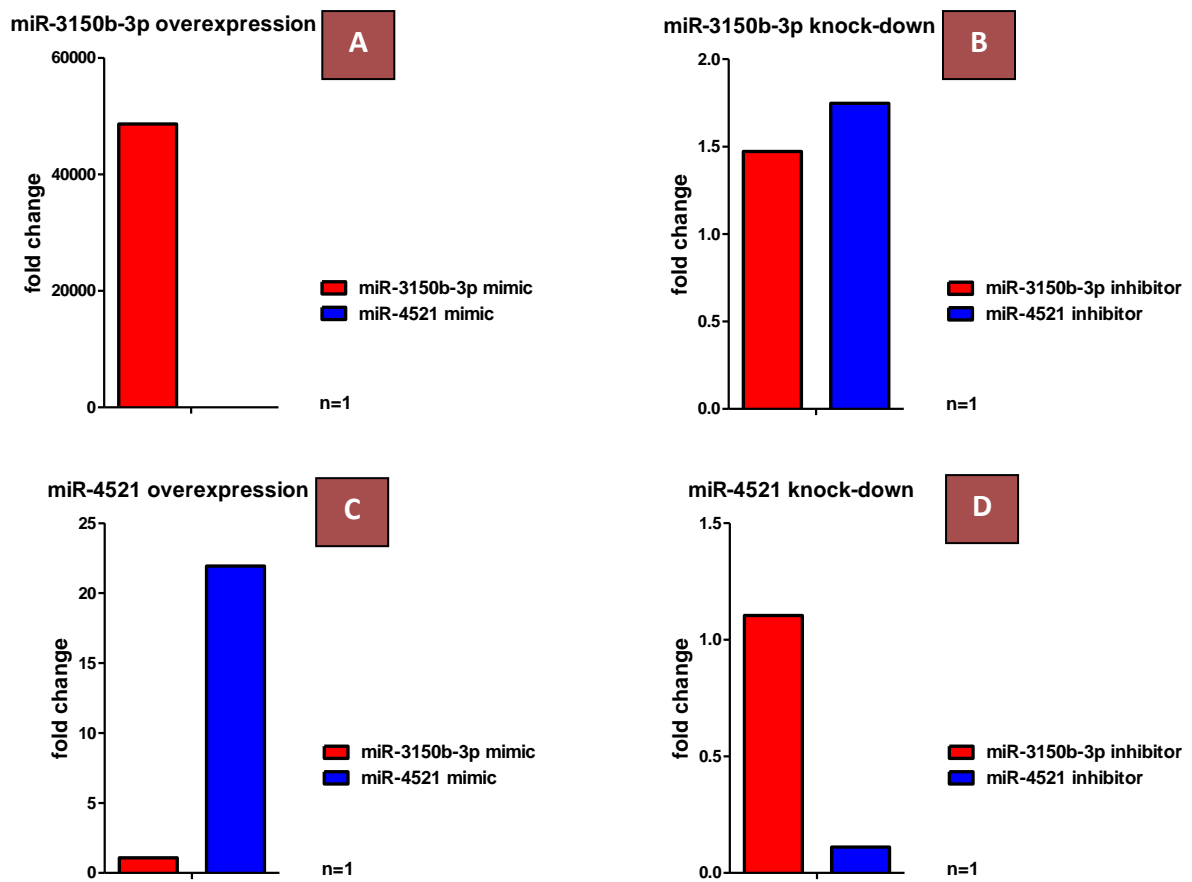


Figure 7: Transfection efficiency of mimics and inhibitors in HUVEC. HUVEC were transfected with (A-B) miR-3150b-3p and (C-D) miR-4521 (A and C) mimics and (B and D) inhibitors to further analyze the efficiency of transfection with real-time qPCR. Both miRNAs were significantly overexpressed while only miR-4521 was successfully knocked down.

5.4 Effect of miRNA mimics and inhibitors on proliferation

To assess whether miR-3150b-3p and miR-4521 mimics as well as inhibitors influence cellular growth a WST-1 metabolic proliferation assay was conducted in the TNBC cell lines BT-549 (Figure 9), MDA-MB-231 (Figure 10), and SUM159 (Figure 11). Therefore, cells were reverse transfected in 96-well plates and incubated for 24-96 hours, and 24-120 hours in two independent experiments.

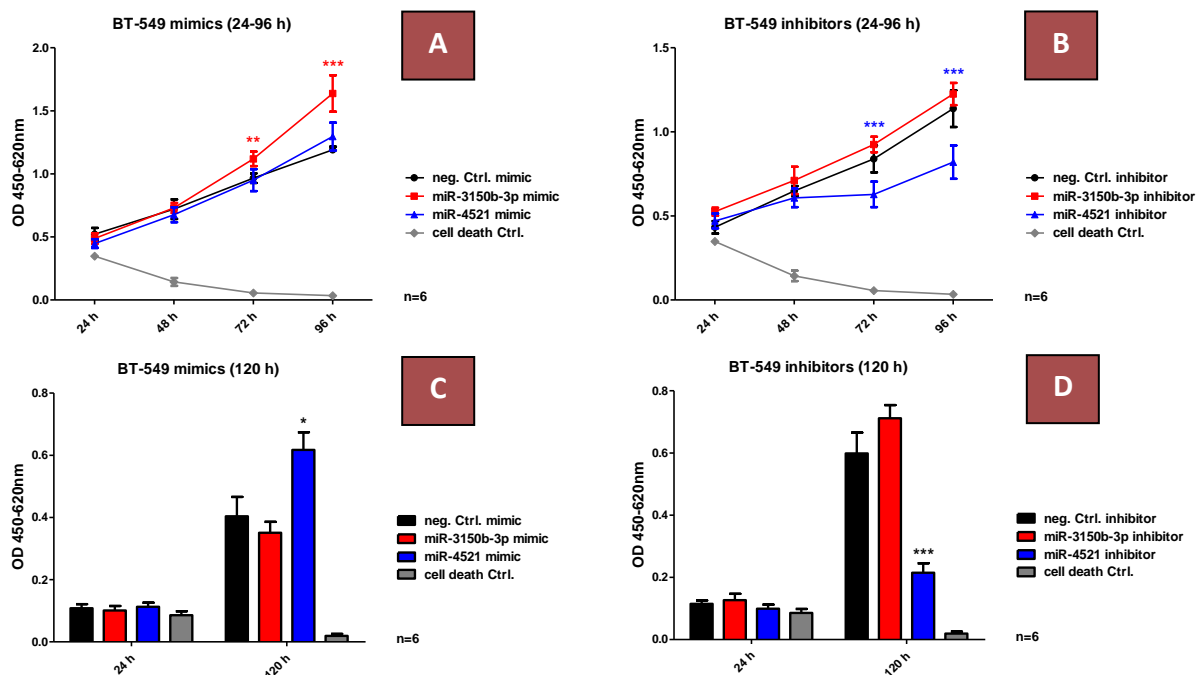


Figure 8: WST-1 metabolic proliferation assay with mimics and inhibitors in BT-549. BT-549 were transfected with miR-3150b-3p and miR-4521 (**A and C**) mimics, (**B and D**) inhibitors, and the cell death control to analyze their effect on cellular growth after (**A-B**) 24-96 h as well as (**C-D**) 24 and 120 h. The miR-3150b-3p mimic increased cell growth after 96 hours and the miR-4521 inhibitor led to a decrease after 72 hours. Significance was determined by one-way ANOVA with Dunnett post-test ($p \leq 0.05 = *$, $0.01 = **$, $0.001 = ***$).

MiR-3150b-3p mimic led to a significant increase in cell growth after 72 hours of incubation. The effect got more pronounced after 96 hours. However, after 120 hours there was a decrease in cell growth. The inhibitor showed no difference compared to the negative control after 96 hours, but the absorbance was slightly increased after 120 hours. The mimic and inhibitor for miR-4521 led to opposite effects in BT-549 (Figure 9). Although, only minor differences were observed between the negative control and mimic after 96 h, cell number increased significantly after 120 hours. The negative effect of the inhibitor was already strong after 72 hours and decreased the cell number even more after 120 hours.

In MDA-MB-231 and SUM159 the results were nearly the same as in BT-549 for miR-3150b-3p after 24-96 hours. A significant increase in cell number was obtained after 48-96 hours in MDA-MB-231 and after 72-96 hours in SUM159. However, the effect of the mimic did not raise after of 120 hours. The miR-3150b-3p inhibitor had no effect (Figure 10B) to a significant increase (Figure 11B). No differences were observed after 120 hours compared to

the negative control. Cell growth was significantly higher in miR-4521 mimic transfected SUM159 after 96 hours. However, there was no difference in MDA-MB-231 cells.

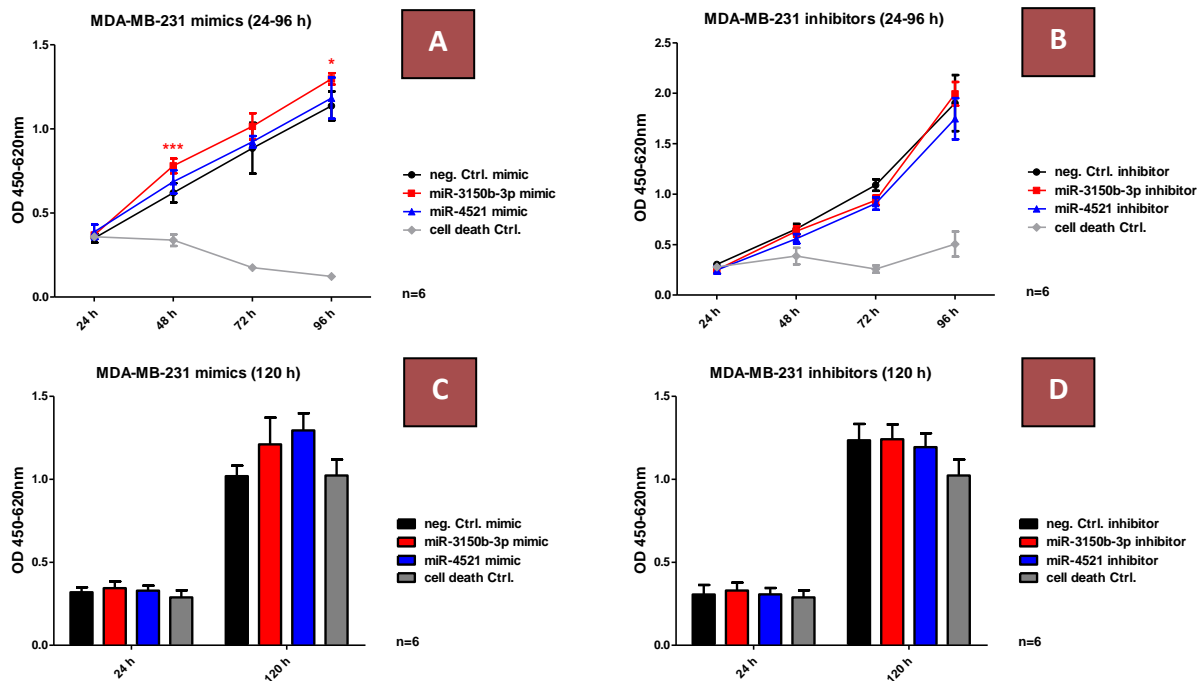


Figure 9: WST-1 metabolic proliferation assay with mimics and inhibitors in MDA-MB-231. MDA-MB-231 were transfected with miR-3150b-3p and miR-4521 (A and C) mimics, (B and D) inhibitors, and the cell death control to analyze their effect on cell growth after (A-B) 24-96 h as well as (C-D) 24 and 120 h. The miR-3150b-3p mimic led to an increase in cellular growth after 48 and 96 hours. Significance was determined by one-way ANOVA with Dunnett post-test ($p \leq 0.05 = *$, $0.01 = **$, $0.001 = ***$).

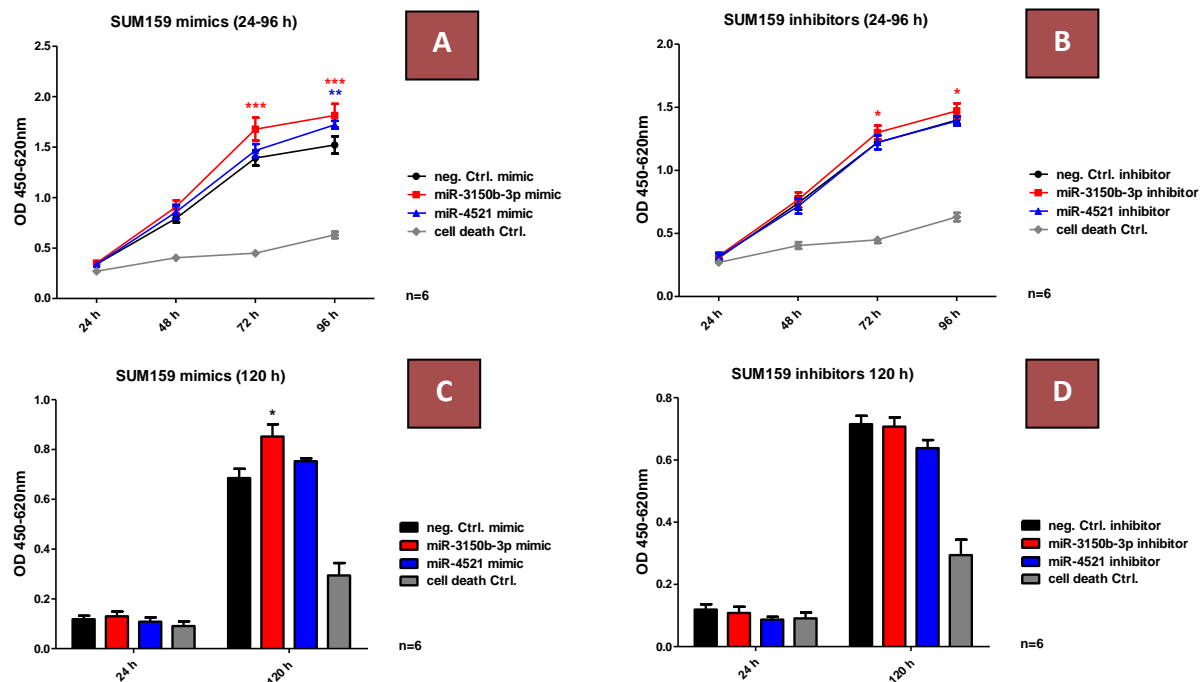


Figure 10: WST-1 metabolic proliferation assay with mimics and inhibitors in SUM159. SUM159 were transfected with miR-3150b-3p and miR-4521 (A and C) mimics, (B and D) inhibitors, and the cell death control to analyze their effect on cell growth after (A-B) 24-96 h as well as (C-D) 24 and 120 h. Both miRNAs led to a significant increase in cell growth after 96 h. Also the miR-3150b-3p inhibitor showed an increase. Significance was determined by one-way ANOVA with Dunnett post-test ($p \leq 0.05 = *$, $0.01 = **$, $0.001 = ***$).

5.5 Differences in colony formation in transfected breast cancer cell lines

The ability of single cells to form colonies and their proliferative activity was analyzed in a CFU assay. Additionally, it was used to see whether cells show the same behavior as in the WST-1 metabolic proliferation assay (mimic = or increased number of colonies, inhibitor = no difference (miR-3150b-3p inhibitor) or decreased number of colonies (miR-4521 inhibitor). Therefore, cells were stained with crystal violet after 16 days (BT-549, Figure 11), 17 days (MDA-MB-231, Figure 12), and 10 days (SUM159, Figure 13). Afterwards, the number of colonies was determined manually.

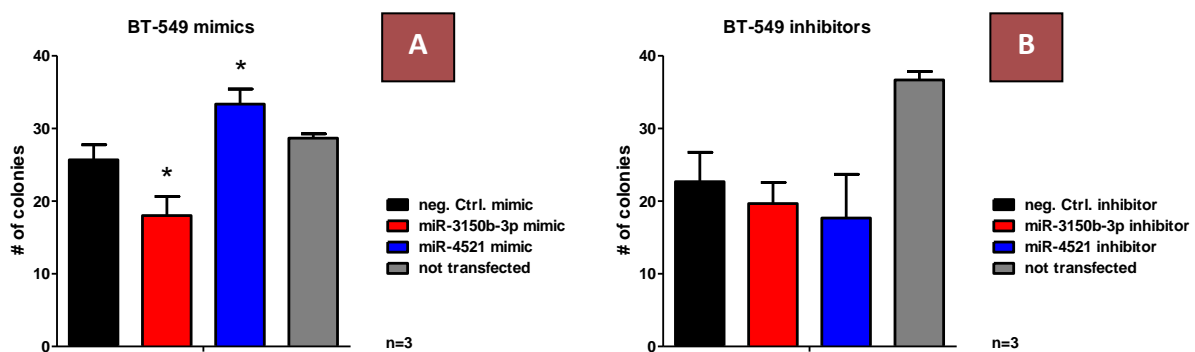


Figure 12: CFU assay with mimics and inhibitors in BT-549. BT-549 were transfected with miR-3150b-3p and miR-4521 (A) mimics and (B) inhibitors to analyze their effect on colony formation. Number of colonies decreased and increased significantly with the miR-3150b-3p and miR-4521 mimics. Significance was determined by one-way ANOVA with Dunnett post-test ($p \leq 0.05 = *$, $0.01 = **$, $0.001 = ***$).

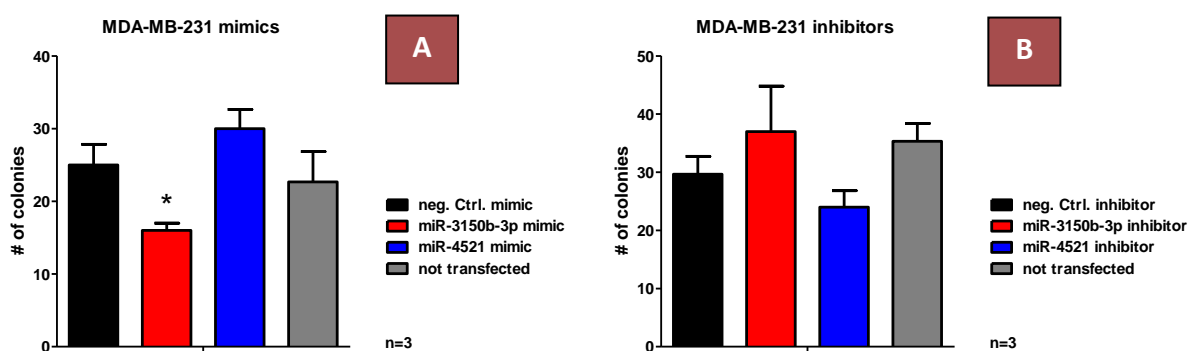


Figure 11: CFU assay with mimics and inhibitors in MDA-MB-231. MDA-MB-231 were transfected with miR-3150b-3p and miR-4521 (A) mimics and (B) inhibitors to analyze their effect on colony formation. The miR-3150b-3p led to a significant increase in colony formation. Significance was determined by one-way ANOVA with Dunnett post-test ($p \leq 0.05 = *$, $0.01 = **$, $0.001 = ***$).

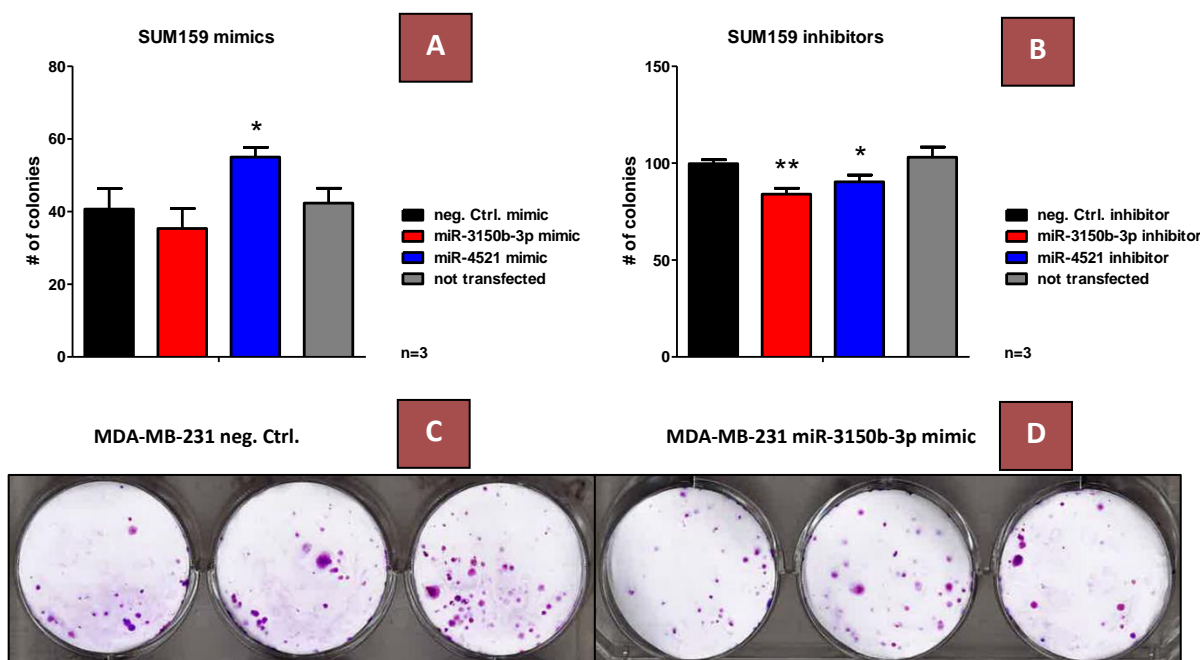


Figure 13: CFU assay with mimics and inhibitors in SUM159 and MDA-MB-231. SUM159 and MDA-MB-231 were transfected with miR-3150b-3p and miR-4521 (**A**, **C**, and **D**) mimics and (**B**) inhibitors to analyze their effect on colony formation. (**A-B**) The miR-4521 mimic enhanced colony formation and both inhibitors showed a decrease. Significance was determined by one-way ANOVA with Dunnett post-test ($p \leq 0.05 = *$, $0.01 = **$, $0.001 = ***$). (**C-D**) Representative images of the stained colonies after 17 days.

The data obtained showed that the miR-3150b-3p mimic lead to a significant decrease in colony formation in BT-549 as well as in MDA-MB-231, and to a slight decrease in SUM159. However, also the inhibitor reduced the number of colonies in two of three cell lines. Colony formation was significantly higher in miR-4521 mimic transfected BT-549 and SUM159. MDA-MB-231 colonies were only slightly increased. In contrast, miR-4521 inhibitor reduced colony formation significantly in SUM159 and minor decreases were obtained in BT-549 as well as MDA-MB-231.

5.6 Influence of miR-4521 on cell cycle progression in BT-549

In a third experiment concerning proliferation it was assessed if the increased and decreased proliferative behavior obtained in the WST-1 metabolic proliferation and the CFU assay resulted from higher cell cycle progression. Therefore, BT-549 cells were transfected with miR-4521 mimic and inhibitor. Additionally, not transfected cells were harvested at optimal density, and high density. Furthermore, one sample included starved cells. The not

transfected and starved cells were used as controls. The amount of DNA was analyzed via PI staining. For evaluation ModFit LT was used.

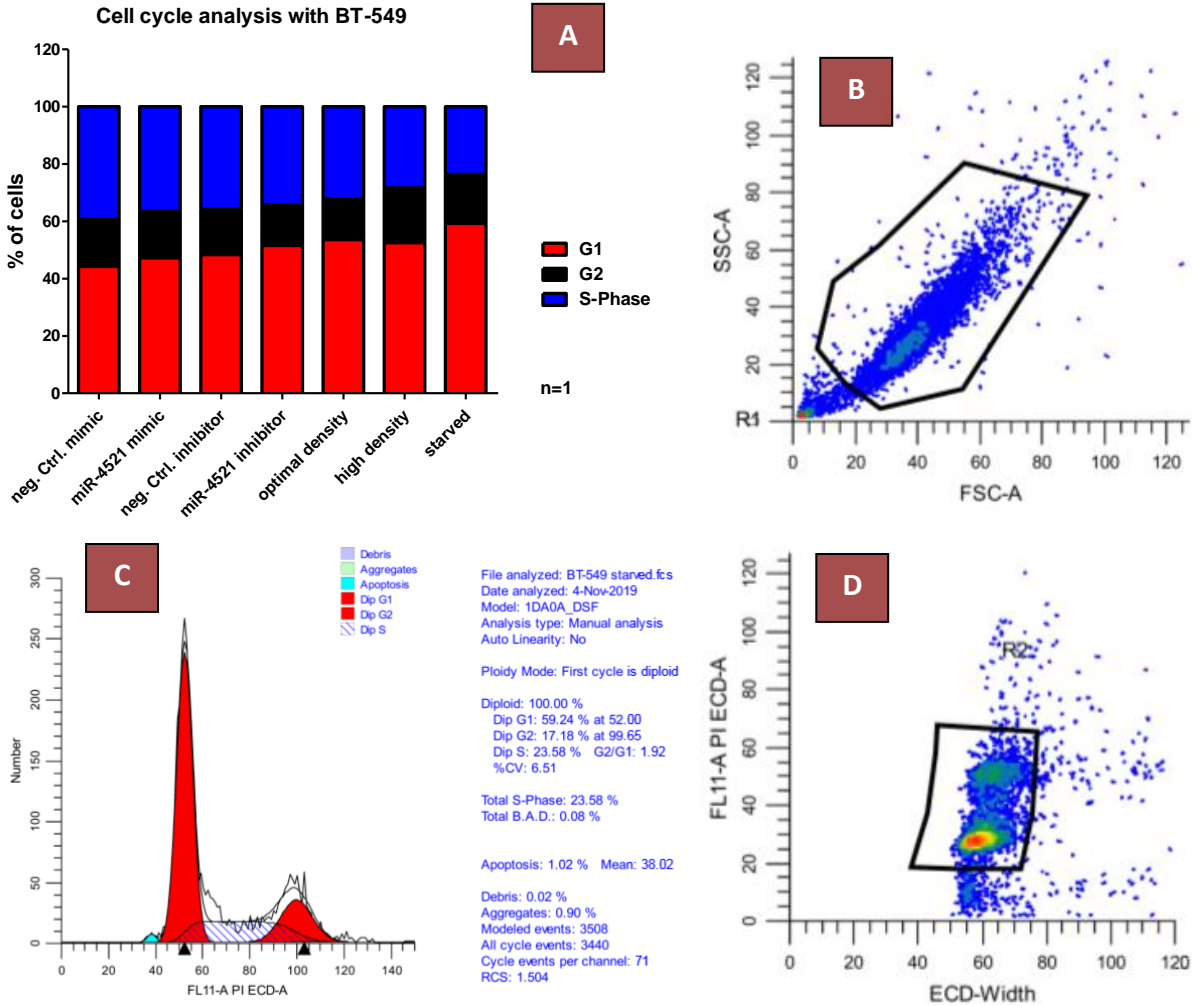


Figure 14: Cell cycle analysis in transfected BT-549 with PI staining. BT-549 were transfected with miR-4521 mimic and inhibitor to analyze their effect on cell cycle progression. Not transfected cells were harvested under optimal, highly confluent, and starved conditions as control. **(A)** Percentage of cells in G₁, G₂, and S phase is depicted in a bar chart with no differences in cell cycle progression compared to the controls. **(C)** Data output from the starved control is shown. **(B and D)** The gating was chosen to exclude cell debris and aggregates.

Focusing on the controls the results show that cells at optimal density (32.10%) seem to be only slightly more in S than cells at high confluence (28.32%). Progression through G₁/S is only inhibited in the starved control (23.58%). MiR-4521 mimic (36.38%) and inhibitor (34.15%) both lead to a slight decrease in the G₁/S transition compared to their negative controls (39.36%, 35.76%). The results could not be statistically evaluated as only one replicate was performed.

5.7 Stimulation of apoptosis in TNBC cell lines

Whether the effects on cellular growth are explainable by induction of apoptosis, we performed a Caspase 3/7 assay. Thus, BT-549 (Figure 15), MDA-MB-231 (Figure 16), and SUM159 (Figure 17) were transfected only with miR-4521 mimic and inhibitor as the results for miR-3150b-3p were contradictory between the WST-1 and CFU assay. The absorbance was measured after 48 hours and 72 hours.

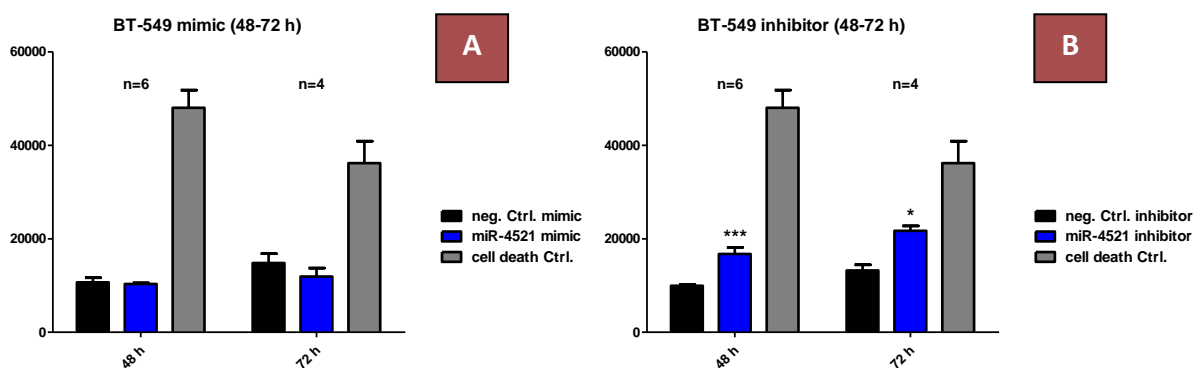


Figure 16: Caspase-GLO™ 3/7 assay with miR-4521 mimic and inhibitor in BT-549. BT-549 were transfected with miR-4521 (A) mimic and (B) inhibitor to analyze their effect on colony formation. A significant increase in apoptosis was observed with the miR-4521 inhibitor. Significance was determined by Mann Whitney test ($p \leq 0.05 = *$, $0.01 = **$, $0.001 = ***$).

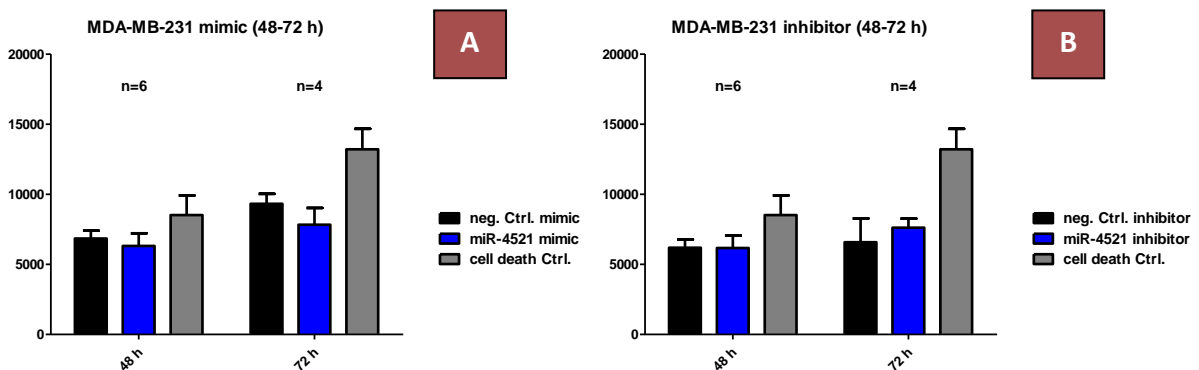


Figure 15: Caspase-GLO™ 3/7 assay with miR-4521 mimic and inhibitor in MDA-MB-231. MDA-MB-231 were transfected with miR-4521 (A) mimic and (B) inhibitor to analyze their effect on colony formation. No differences were observed in MDA-MB-231. Significance was determined by Mann Whitney test ($p \leq 0.05 = *$, $0.01 = **$, $0.001 = ***$).

Out of all three cell lines investigated BT-549 was the only one to show significantly increased apoptosis after 48 h and 72 h when transfected with the miR-4521 inhibitor. Transfection of MDA-MB-231 and SUM159 with either mimic or inhibitor did not result in any differences in apoptotic activity compared to the negative control.

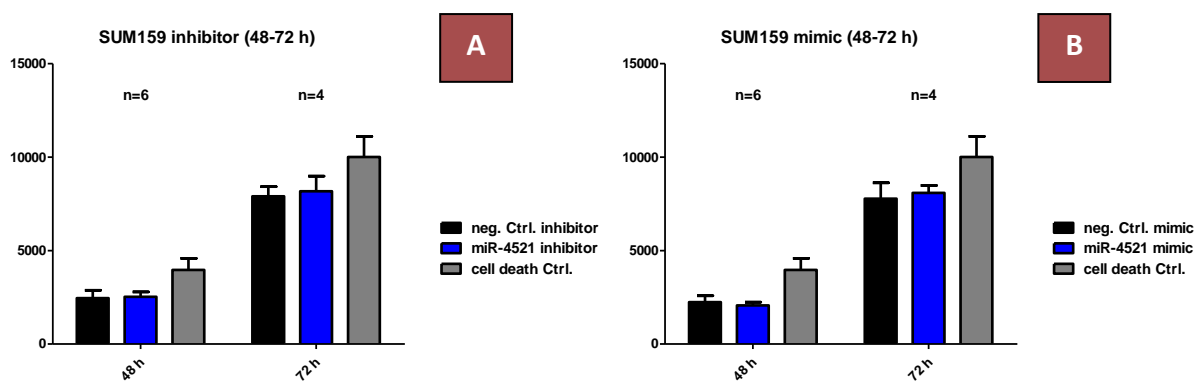


Figure 17: Caspase-GLO™ 3/7 assay with miR-4521 mimic and inhibitor in SUM159. SUM159 were transfected with miR-4521 (A) mimic and (B) inhibitor to analyze their effect on colony formation. No differences were observed in SUM159. Significance was determined by Mann Whitney U test ($p \leq 0.05 = *$, $0.01 = **$, $0.001 = ***$).

5.8 Expression levels of two cell cycle markers under the influence of miR-4521

The RNA isolated from transfected BT-549 was used to investigate the expression levels of two key players in cell cycle progression, namely cyclin D1 and RAD1 which encodes a protein of the 9-1-1 complex. To do so, specific primer for these two genes and GAPDH as housekeeper were used for real-time qPCR analysis.

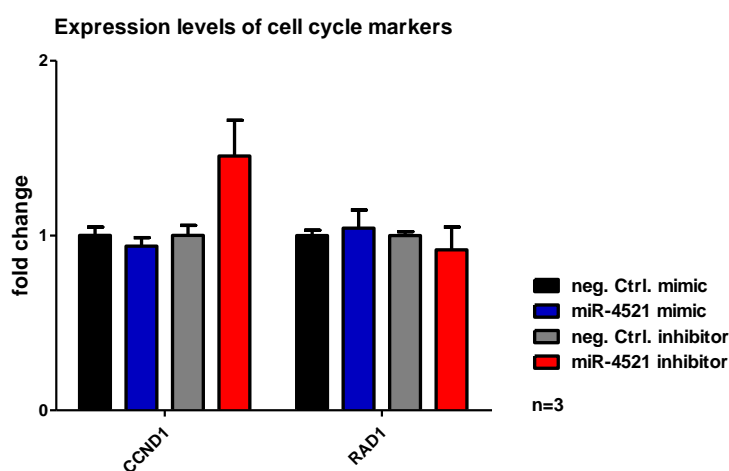


Figure 18: Expression levels of cyclin D1 and RAD1 in transfected BT-549. BT-549 were transfected with miR-4521 mimic and inhibitor to further analyze their influence on these two genes with real-time qPCR. A slight increase in CCND1 expression level was observed. Significance was determined by Mann Whitney U test ($p \leq 0.05 = *$, $0.01 = **$, $0.001 = ***$). CCND1=cyclin D1.

It was observed that the miR-4521 mimic did not result in any differential expression of the two target genes. However, the inhibitor slightly up-regulated cyclin D1, but did also not affect RAD1 expression level.

5.9 MiR-3150b-3p and miR-4521 influence tube formation in HUVEC

Moreover, it was assessed in the tube formation assay using HUVEC if miR-3150b-3p and miR-4521 are capable of promoting or inhibiting angiogenesis. After calcein staining the formed tubes were imaged and evaluated in ImageJ.

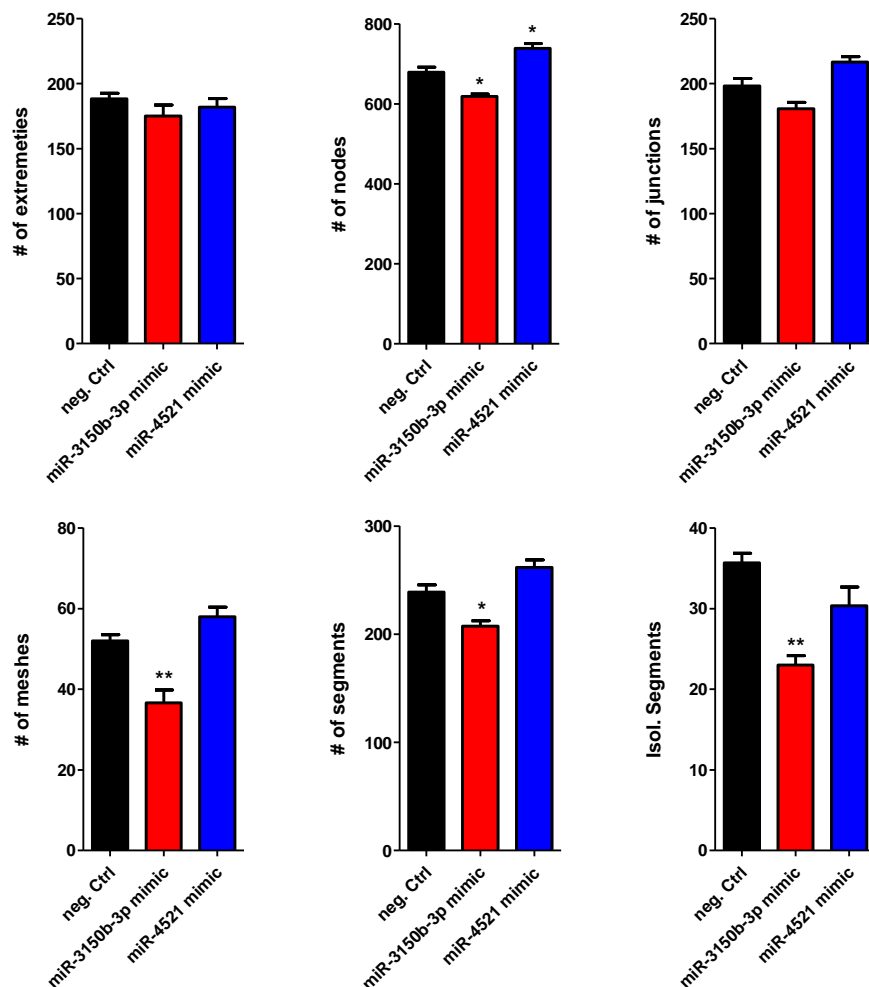


Figure 19: Tube formation assay with HUVEC and miRNA mimics. HUVEC were transfected with miR-3150b-3p and miR-4521 mimics to analyze their effect on tube formation. The number of nodes, meshes, segments, and isolated segments were significantly decreased in miR-3150b-3p transfected cells. The miR-4521 mimic led to a significant increase in the number of nodes. Significance was determined by one-way ANOVA with Dunnett post-test ($p < 0.05 = *$, $0.01 = **$, $0.001 = ***$).

The transfection with the miR-3150b-3p mimic inhibited tube formation significantly regarding the parameters number of nodes, meshes, and segments, and isolated segments. The miR-4521 mimic showed a significant increase only in the number of nodes. The other parameters were slightly increased except the isolated segments.

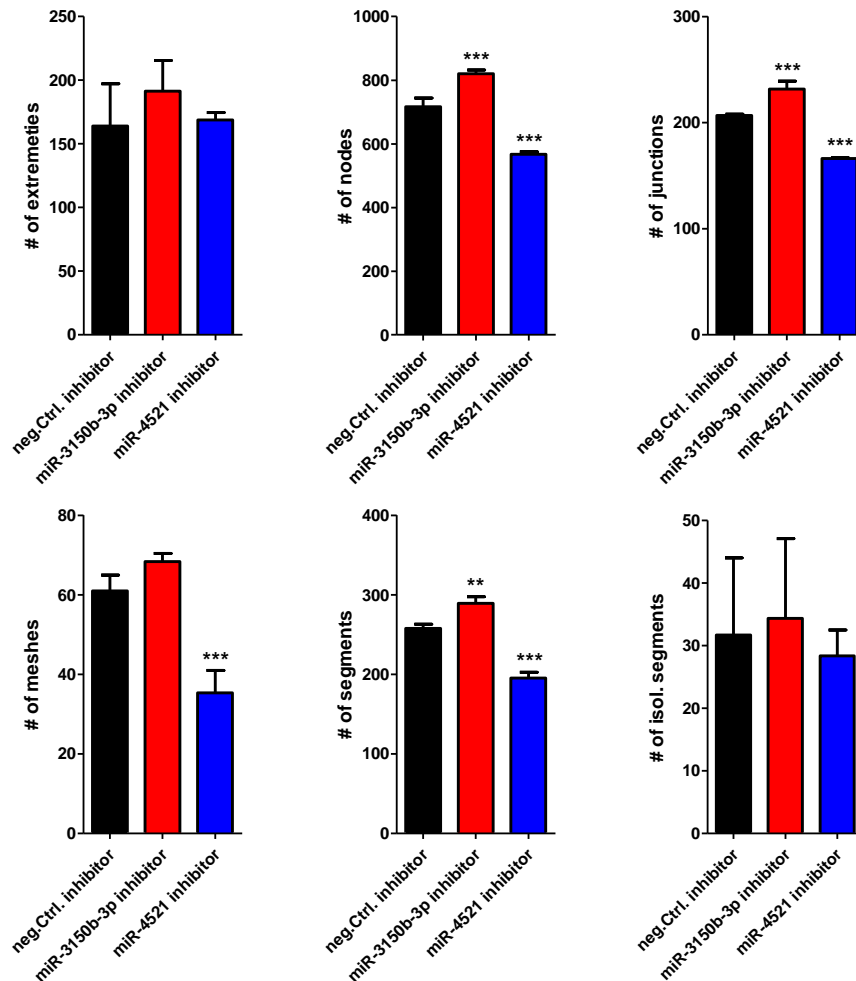


Figure 20: Tube formation assay with HUVEC and miRNA inhibitors. HUVEC were transfected with miR-3150b-3p and miR-4521 inhibitors to analyze their effect on tube formation. The number of nodes, junctions, and segments was significantly increased after transfection with the miR-3150b-3p inhibitor. The miR-4521 inhibitor led to a significant decrease in the number of nodes, junctions, meshes, and segments. Significance was determined by one-way ANOVA with Dunnett post-test ($p \leq 0.05 = *$, $0.01 = **$, $0.001 = ***$).

MiRNA inhibitors resulted in the opposite effects seen in the experiment with the mimics. The miR-3150b-3p inhibitor promoted tube formation significantly regarding the number of nodes, junctions, and segments. Although, miR-4521 mimic did not result in significant increases looking at most of the parameters, the inhibitor decreased the number nodes, junctions, meshes, and segments significantly.

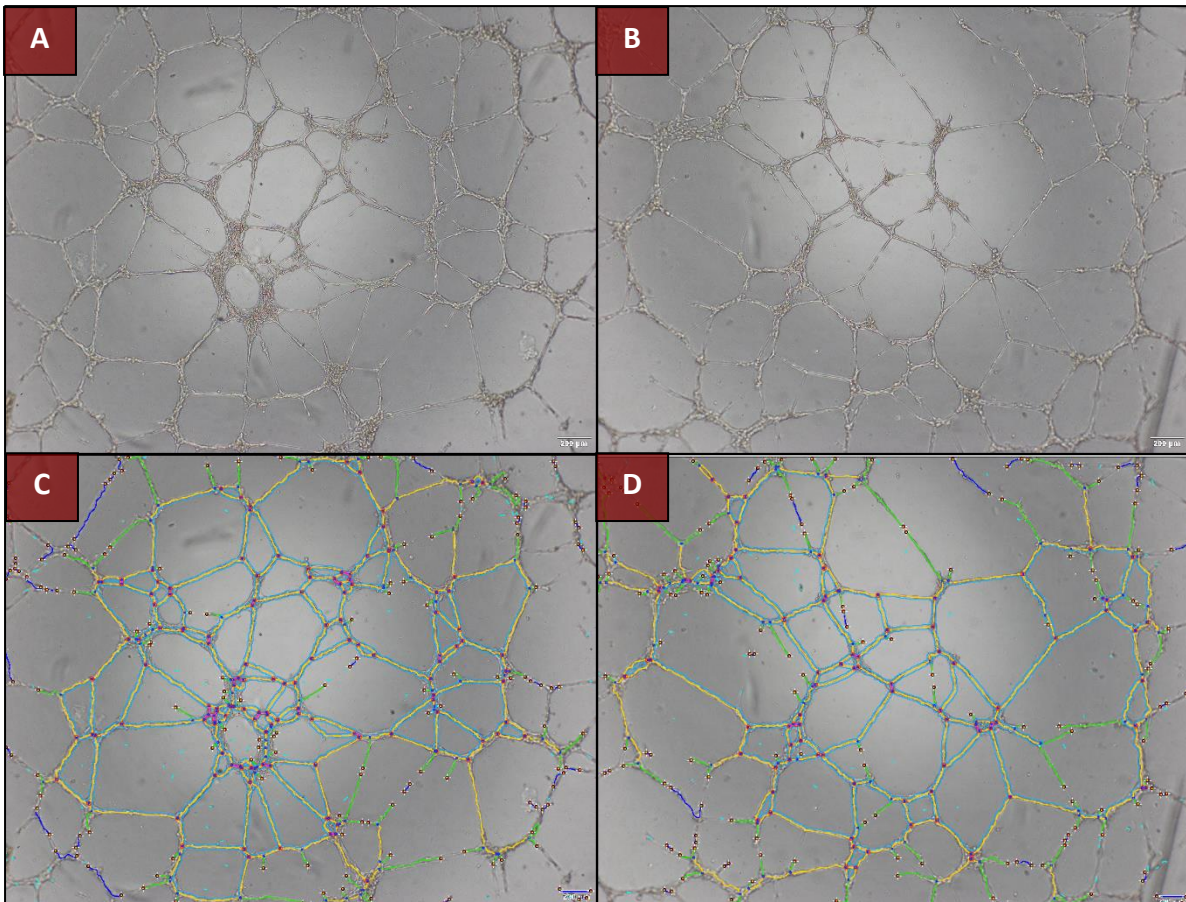


Figure 21: Tube formation assay. The images were taken with transmitted light and show the **(A)** negative control, and **(B)** miR-4521 inhibitor. **(C-D)** ImageJ evaluates different parameters of tube formation by using specific algorithms.

5.10 Angiogenesis related gene expression influenced by miR-4521

The RNA isolated from transfected BT-549 was used to investigate the expression levels of angiogenesis related genes. To do so, specific primer for the target genes and GAPDH as housekeeper were used for real-time qPCR analysis.

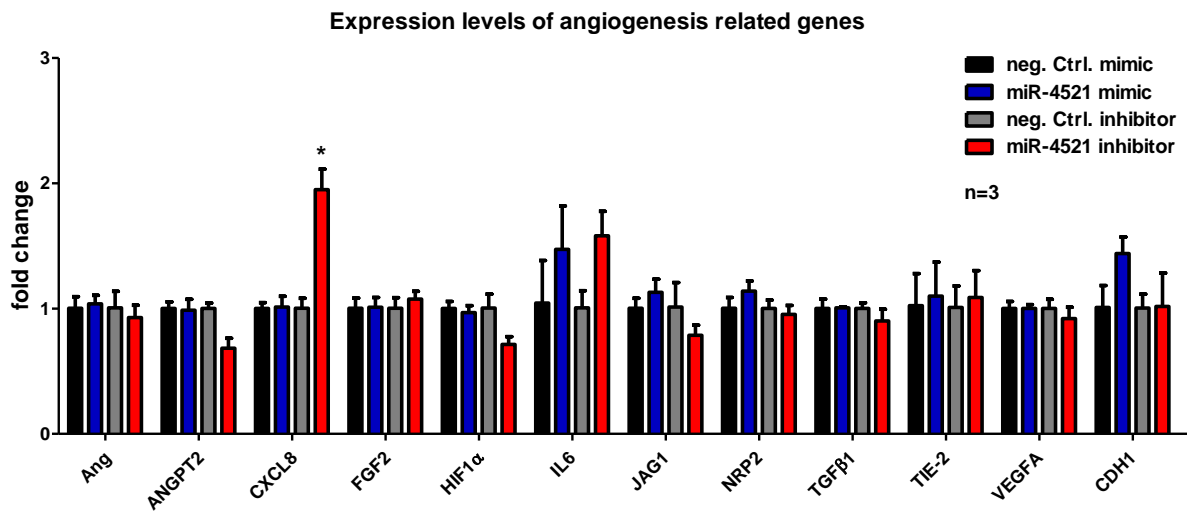


Figure 22: Expression levels of angiogenesis related genes in transfected BT-549. BT-549 were transfected with miR-4521 mimic and inhibitor to further analyze their influence on target genes important for angiogenesis with real-time PCR. CXCL8 expression level was significantly increased in BT-549. Significance was determined by Mann Whitney U test ($p < 0.05 = *$, $0.01 = **$, $0.001 = ***$). Ang=Angiogenin, ANGPT2=Angiopoietin 2, CXCL8=C-X-C Motif Chemokine Ligand 8, FGF2=Fibroblast Growth Factor 2, HIF1 α =Hypoxia Inducible Factor 1 Subunit α , IL6=Interleukin 6, JAG1=Jagged Canonical Notch Ligand 1, NRP2=Neuropilin 2, TGF β 1=Transforming Growth Factor β 1, TIE-2=Tyrosine Kinase with Immunoglobulin like and EGF like Domains 2, VEGFA=Vascular Endothelial Growth Factor A, CDH1=Cadherin 1.

The results obtained show that miR-4521 mimic led to a slight increase in only one of the genes namely CDH1. The inhibitor led to minor decreases in ANGPT2, HIF1 α , and JAG1 expression levels. Moreover, IL6 expression was slightly and CXCL8 expression significantly elevated. Within the genes Ang, FGF2, NRP2, TGF β 1, TIE-2, and VEGFA no differences could be observed.

6 Discussion

In this study, two novel miRNAs identified in the work of Schwarzenbacher et al. 2019 were used for *in vitro* expression analyses, manipulation, and downstream assays. MiR-3150b-3p and miR-4521 were shown to be significantly up- and down-regulated in breast cancer tissues compared to surrounding normal tissue. Therefore, they were considered to play a role in the initiation and progression of breast cancer.

In the KM plotter it was obtained that a higher expression of miR-3150b-3p would result to a worse outcome after 60 months follow-up in all breast cancer subtypes and TNBC specifically which confirms the results from Schwarzenbacher et al. 2019. However, high expression levels of miR-4521 seem to lead to a shorter OS regarding all subtypes although it was found to be down-regulated in tumorous tissue. This might be since different datasets were used. Additionally, not only tumour cells were analyzed but also cells of the surrounding healthy tissue which influence the gene expression and lead to changes between different studies. OS curves were also generated considering only TNBC for miR-4521 where a low expression led to a worse outcome. However, the sample size was rather small (n=97) and the plot could change when analysis more samples. Altogether, these data suggest that both miRNAs show clinical relevance in human breast cancer.

Mir-3150b-3p and miR-4521 expression levels were further analyzed in different breast cancer cell lines to explore the expression levels and identify an optimal experimental model system. SNORD61 and SNORD95 were used as reference as they showed the lowest variation across the used breast cancer cell lines. Mir-3150b-3p expression was very low and significantly up-regulated only in HCC1914 (4-fold). In the other cell lines only a slight up- and down-regulation could be observed which is unlike the expression levels observed in patient's tissues. This might be due to influence on gene expression of surrounding cells in primary tumor samples. MiR-4521 was not only higher expressed in patients with worse outcome, but it was additionally observed to be significantly up-regulated in the TNBC cell lines MDA-MB-231 and moderately up-regulated in BT-549 and SUM159. However, these results have to be treated with care, since there is a high variation within the three replicates, especially in SUM159. The high standard deviation could be explained by the instable genome as well as high mutation rate of cancer cells and a resulting change in

expression levels over different passages. However, miR-4521 seemed to be deregulated in the TNBC cell lines BT-549, MDA-MB-231 and SUM159. As breast cancer is a very heterogeneous disease in terms of clinical behavior, prognosis and biology, we decided to focus in our thesis on TNBC.

MiRNA mimics and inhibitors efficiency was tested at the beginning. MiR-4521 was successfully up- and down-regulated with the mimic and inhibitor. Interestingly, miR-4521 mimic seemed to also have an impact on miR-3150b-3p expression. This could be due to the fact that an up-regulation of about 300-fold was achieved for miR-4521 in SUM159 which may lead to off-target effects. However, also the miR-4521 inhibitor resulted in a down-regulation of miR-3150b-3p. This could be explained by the high concentration used for the inhibitor resulting in similar off-target effects. Altogether, only miR-4521 expression was successfully manipulated without side-effects on the other miRNA expression levels. For miR-3150b-3p other expression modulation methods should be considered such as lentiviral transfection or CRIPSR/Cas9. However, mimics and inhibitors for both miRNAs were used for proliferation, and angiogenesis assays.

First, it was focused on the main hallmark of cancer which is excessive proliferation. This was assessed in the WST-1 assay. The data obtained suggest that the miR-3150b-3p mimic leads to a higher cellular growth whereas no effects were seen with the inhibitor. In SUM159 also the inhibitor led to an increase after 72 hours. The missing effects of the inhibitor may result of the already very low endogenous expression of miR-3150b-3p across all breast cancer cell lines why also the knock-down was not successful. MiR-4521 mimic and inhibitor led to higher and lower proliferation respectively. Although, the results were only significant in BT-549 the other cell lines showed the same trend indicating that inhibition of miR-4521 could result in slower tumor growth and progression. Taken together, both miRNAs seemed to alter proliferative behavior when modulated with mimic or inhibitor but miR-3150b-3p could only be up-regulated positively influencing tumour growth.

Subsequently, the aim was to confirm the results in a CFU assay. Yet, miR-3150b-3p modulation in the CFU assay led to opposite results than observed in the WST-1 assay. The mimic resulted in less and the inhibitor in more colonies compared to the negative controls. This assay comprises not only cellular growth but also the ability of single cells to form colonies which might be the reason why the CFU and the WST-1 assay led to different results. Additionally, the effects of the inhibitor varied across the three cell lines which could have the same reason as in the metabolic proliferation assay. Considering the opposite effects of the mimic in the two assays, and the weak effects of the inhibitor this miRNA was not used for further assays. In contrary, miRNA 4521 mimic led to a higher and the inhibitor to a lower number of colonies confirming the previous results. This further suggests its importance in cellular growth.

In a third experiment it was investigated if cell cycle is shifted by the expression variation of the miRNAs. Unfortunately, as the controls did not result in reliable results they could not be used as an optimal confluency resulted in a lower percentage of cells in S compared to starving. This ambiguity could be due to technical difficulties in the preparation of the staining solution. Therefore, an apoptosis assay was considered to assess whether proliferation is dependent on increased or decreased cell death induction.

The caspase-GLO 3/7 assay resulted in no change in apoptosis when cells were transfected with the mimic. However, the inhibitor seemed to stimulate cell death in BT-549 suggesting that decreased proliferation might be due to an increase in apoptosis. These results cannot be considered as generalizable as only one cell line showed this effect.

In other studies, FAM129A and FOXM1 were shown to be directly targeted by miR-4521 leading to a decrease in downstream signalling. Consequently, overexpression of miR-4521 was already observed to decrease proliferation and migration, and promote cell cycle arrest while leading to an increase in apoptosis in medulloblastoma and clear cell renal cell carcinoma (Feng X. et al. 2019, Senfter D. et al. 2019). Regarding the results obtained in the WST-1 metabolic proliferation, CFU, and apoptosis assay there are discrepancies in our

studies. The opposite outcome could be the result of the investigation of different cancer types as different breast cancer subtypes already show a strong heterogeneity. Additionally, more proliferation markers should be investigated as CCND1 and RAD1 showed no differential expression after mimic and inhibitor treatment.

When tumors grow, they start requiring their own blood supply system at some critical point. Therefore, the effects of miR-3150b-3p and miR-4521 mimics as well as inhibitors on angiogenesis were assessed. The results for miR-3150b-3p indicated that the mimic leads to an inhibition of tube formation which would further result in decreased tumour growth as tumors would lack oxygen and nutrients. Therefore, it seemed that miR-3150b-3p up-regulation could have positive effects in breast cancer regarding the CFU and angiogenesis assay. This was in accordance with the study of Zhang et al. 2019 where miR-3150b-3p was shown to inhibit colorectal cancer progression. MiR-4521 results were again consistent with the others suggesting its tumour promoting role when highly expressed.

In the last experiment also several angiogenesis markers were assessed in real-time qPCR to find a possible target of miR-4521. Only one candidate seemed to be affected by the inhibitor. CXCL8 which is suggested to mediate VEGF signalling (Martin et al. 2009) was shown in this study to be up-regulated upon inhibition of miR-4521 suggesting this gene to be possibly regulated by this miRNA. Therefore, this factor should be further investigated. However, it seemed that in cancer cells the investigated angiogenesis related genes were not deregulated upon transfection although there was an effect in HUVECs. This suggests that miR-4521 acts extracellularly on angiogenesis.

Taken together, the above delineated results suggest that miR-3150b-3p and especially miR-4521 may play an important role in in breast cancer initiation and progression. Conducted experiments need to be repeated and further ones are necessary to fully characterize the function of the miRNAs and to shed light on their effects on various hallmarks of cancer.

Abbreviations

Table 20: Abbreviations

Anaphase-promoting complex or cyclosome	APC/C
Angiopoietin-2	Ang2
Apoptotic protease-activating factor 1	Apaf-1
Argonaute	Ago
B-cell lymphoma 2	Bcl-2
Bcl-2 associated X protein	Bax
Bcl-2 homology	BH
Cdc45-MCM-GINS	CMG
Cdk-activating kinase	CAK
Cell division cycle	Cdc
Chromatin licensing and DNA replication factor 1	Cdt1
Colony forming unit	CFU
Cyclin-dependent kinase	Cdk
DBF4-dependent kinase	DDK
Death-inducing signalling complex	DISC
Decapping protein 2	DCP2
DiGeorge syndrome critical region gene 8	DGCR8
double-strand RNA binding domain	dsRBD
Epidermal growth factor	EGF
Estrogen receptor	ER
Eukaryotic translational initiation factor 4F complex	eIF4G
Exportin 5	EXP5
Fas-associated death domain	FADD
Fetal bovine serum	FBS
Fibroblast growth factor	FGF

Fluorescence-activated cell sorting	FACS
Gap phase	G
Gene stability value	M value
Guanine nucleotide exchange factor	GEF
Guanosine diphosphate	GDP
Guanosine triphosphate	GTP
Hypoxia-inducible factor	HIF
Higher human development index countries	HDI
Hormone receptor	HR
Human epidermal growth factor receptor	HER2/neu
Kaplan-Meyer	KM
MicroRNA	MiRNA
Middle	MID
Minichromosome maintenance	MCM
Mitogen-activated protein kinase	MAPK
Mitosis phase	M
Non-coding RNA	NcRNA
Nuclear pore complexes	NPC
Nucleotide	Nt
Origin recognition complex	ORC
Overall survival	OS
P-element Induced Wimpy testis	PIWI
Phosphate buffered saline	PBS
Piwi/Argonaute/Zwille	PAZ
Platelet-derived growth factor	PDGF
Poly-A binding protein	PABP
Pre-replication complex	Pre-RC
Precursor miRNA	Pre-miRNA
Primary miRNA	Pri-miRNA
Propidium iodide	PI
Progesterone receptor	PR

Ran GTPase-activating protein	RanGAP
Retinoblastoma protein	Rb
Reverse transcriptase	RT
RNA-induced silencing complex	RISC
RNA polymerase II	RNA Pol II
Skp1, Cullin, F-box proteins	SCF
Synthesis phase	S
transforming growth factor- β	TGF- β
Triple negative breast cancer	TNBC
Untranslated region	UTR
Vascular endothelial growth factor	VEGF
Exoribonuclease 1	Xrn1p
1-bromo-3-chloropropane	BCP

References

- Akram, M. et al., 2017. Awareness and current knowledge of breast cancer. *Biological Research*. 50:33.
- Alberts, B. et al., 2015. *Molecular Biology of the Cell* (Sixth edition). *Garland Science*. pp.
- American Cancer Society. *Breast Cancer Facts & Figures 2017-2018*. *Atlanta: American Cancer Society, Inc.* 2017.
- Aprelikova, O. et al., 1995. Both p16 and p21 Families of Cyclin-dependent Kinase (CDK) Inhibitors Block the Phosphorylation of Cyclin-dependent Kinases by the CDK-activating Kinase. *The Journal of Biological Chemistry*. pp. 18195-18197.
- Aysola, K. et al., 2013. Triple Negative Breast Cancer - An Overview. *Hereditary Genetics*. doi:10.4172/2161-1041.S2-001.
- Bell, S. P. & Stillman, B., 1992. ATP-dependent recognition of eukaryotic origins of DNA replication by a multi-protein complex. *Nature*. pp. 128-134.
- Bertoli, C. et al., 2013. Control of cell cycle transcription during G1 and S phases. *Nature Reviews Molecular Cell Biology*. pp. 518-528.
- Bray, F. et al., 2018. Global Cancer Statistics 2018: GLOBOCAN Estimates of Incidence and Mortality Worldwide for 36 Cancers in 185 Countries. *Cancer Journal for Clinicians*. pp. 394-424.
- Breast Cancer Incidence and Mortality. *Statistik Austria*. Available at: http://www.statistik-austria.at/web_de/statistiken/menschen_und_gesellschaft/gesundheit/krebserkrankungen/brust/index.html. [Accessed September 10.2019].
- Bryant, J. A. & Aves, S. J., 2011. Initiation of DNA replication: functional and evolutionary aspects. *Annals of Botany*. pp. 1119-1126.
- Cairrão, F. & Domingo, P. M., 2010. Apoptosis: Molecular Mechanisms. *Encyclopedia of Life Sciences*. DOI: 10.1002.

Cerami et al., 2012. The cBio Cancer Genomics Portal: An Open Platform for Exploring Multidimensional Cancer Genomics Data. *Cancer Discovery*. p. 401.

Duronio, R. J. & Xiong, Y., 2013. Signaling Pathways that Control Cell Proliferation. *Cold Spring Harbor Perspectives in Biology*. 5:a008904.

Evan, G. I. & Vousden K. H., 2001. Proliferation, cell cycle and apoptosis in cancer. *Nature*. pp. 342-348.

Evan, G. & Littlewood, T., 1998. A Matter of Life and Cell Death. *Science*. pp. 1317-1321.

Elmore, S., 2007. Apoptosis: A Review of Programmed Cell Death. *Toxicologic Pathology*. pp. 495-516.

Feng, X. et al., 2019. miR-4521-FAM129A axial regulation on ccRCC progression through TIMP-1/MMP2/MMP9 and MDM2/p53/Bcl2/Bax pathways. *Cell Death Discovery*. 5:89.

Frigola, J. et al., 2016. Cdt1 stabilizes an open MCM ring for helicase loading. *Nature Communications*. DOI: 10.1038.

Fukuhara, S. et al., 2010. Angiopoietin-1/Tie2 receptor signaling in vascular quiescence and angiogenesis. *Histology and Histopathology*. pp. 387-396.

Gao et al., 2013. Integrative analysis of complex cancer genomics and clinical profiles using the cBioPortal. *Science Signaling* 6. p11.

Gupta, M. K. & Qin, R. Y., 2003. Mechanism and its regulation of tumor-induced angiogenesis. *World Journal of Gastroenterology*. pp. 1144-1155.

Hanahan, D. & Weinberg, R. A., 2011. Hallmarks of Cancer: The Next Generation. *Cell*. DOI 10.1016.

Hellemans, J. et al., 2007. qBase relative quantification framework and software for management and automated analysis of real-time quantitative PCR data. *Genome Biology*. DOI: 10.1186.

https://www.cbioportal.org/study/summary?id=brca_metabric%2Cbrca_tcga_pub2015.
[Accessed December 25.2019].

- Jansson, M. D. & Lund, A. H., 2012. MicroRNA and cancer. *Molecular Oncology* 6. pp. 590-610.
- Karamysheva, A. F., 2008. Mechanisms of Angiogenesis. *Biokhimiya*. pp. 935-948.
- Khan, S. et al., 2019. MicroRNA biogenesis, gene silencing mechanisms and role in breast, ovarian and prostate cancer. *Biochimie*. 12–24.
- Khan, F. et al., 2018. Expression of p27 and c-Myc by immunohistochemistry in Breast Ductal Cancers in African American Women. *Annals of Diagnostic Pathology*. pp. 170-174.
- Kwak, P. B. & Tomari, Y., 2012. The N domain of Argonaute drives duplex unwinding during RISC assembly. *Nature Structural & Molecular Biology*. doi:10.1038/nsmb.2232.
- Lau, P. W. et al., 2012. The Molecular Architecture of Human Dicer. *Nature Structural & Molecular Biology*. pp. 436-440.
- Lin S. & Gregory R. I., 2015. MicroRNA biogenesis pathways in cancer. *Nature Reviews Cancer* 15. pp. 321-333.
- Lodish, H. et al., 2012. Molecular Cell Biology (Seventh edition). *W. H. Freeman and Company*. pp.
- Lowe, S. W. et al., 2004. Intrinsic tumour suppression. *Nature*. pp. 307-315.
- Luo, L. et al., 2018. Decreased miR-320 expression is associated with breast cancer progression, cell migration, and invasiveness via targeting Aquaporin 1. *Oxford University Press*. pp. 473-480.
- MacFarlane, L. A. & Murphy, P. R., 2010. MicroRNA: Biogenesis, Function and Role in Cancer. *Current Genomics*. pp. 537-561.
- Martin, D. et al., 2009. CXCL8/IL8 Stimulates Vascular Endothelial Growth Factor (VEGF) Expression and the Autocrine Activation of VEGFR2 in Endothelial Cells by Activating NFκB through the CBM (Carma3/Bcl10/Malt1) Complex. *Journal of Biological Chemistry*. pp. 6038-6042.
- Moiseeva, T. N. & Bakkenist, C. J., 2018. Regulation of the initiation of DNA replication in human cells. *DNA Repair (Amst)*. pp. 99-106.

- Momenimovahed, Z. & Salehiniya, H., 2019. Epidemiological characteristics of and risk factors for breast cancer in the world. *Breast Cancer - Targets and Therapy*. pp. 151-164.
- Murray, A. W., 2004. Recycling the Cell Cycle: Cyclins Revisited. *Cell*. pp. 221-234.
- Papetti, M. & Herman, I. M., 2002. Mechanisms of normal and tumor-derived angiogenesis. *American Journal of Physiology-Cell Physiology*. pp. 947-970.
- Prat, A. et al., 2015. Clinical implications of the intrinsic molecular subtypes of breast cancer. *The Breast* 24. pp. 26-35.
- Reed, J. C., 2000. Mechanisms of Apoptosis. *American Journal of Pathology*. pp. 1415-1430.
- Risau, W., 1997. Mechanisms of angiogenesis. *Nature*. pp. 671-674.
- Schneeweiss, A. et al., 2019. Diagnosis and Therapy of Triple-Negative Breast Cancer (TNBC) – Recommendations for Daily Routine Practice. *Geburtshilfe und Frauenheilkunde*. pp. 605-617.
- Schwarzenbacher, D., 2019. MiR-1287-5p inhibits triple negative breast cancer growth by interaction with phosphoinositide 3-kinase CB, thereby sensitizing cells for PI3Kinase inhibitors. *Breast Cancer Research*. 21:20.
- Senfter, D. et al., 2019. High impact of miRNA-4521 on FOXM1 expression in medulloblastoma. *Cell Death & Disease*. 10:696.
- Sherr, C. J. & Roberts J. M., 2019. CDK inhibitors: positive and negative regulators of G₁-phase progression. *Genes & Development*. pp. 13:1501-1512.
- Siddiqui, K. & Stillman, B., 2007. ATP-dependent Assembly of the Human Origin Recognition Complex. *The Journal of Biological Chemistry*. pp. 32370–32383.
- Teichert, M. et al., 2017. Pericyte-expressed Tie2 controls angiogenesis and vessel maturation. *Nature Communications*. DOI: 10.1038.
- Thurston, G. & Daly, C., 2012. The Complex Role of Angiopoietin-2 in the Angiopoietin-Tie Signaling Pathway. *Cold Spring Harbor Perspectives in Medicine*. 2:a006650.

Wan, P. T. C. et al., 2004. Mechanism of Activation of the RAF-ERK Signaling Pathway by Oncogenic Mutations of B-RAF. *Cell*. pp. 855-867.

Witsch, E. et al., 2010. Roles for Growth Factors in Cancer Progression. *Physiology*. pp. 85-101.

Yeeles, J. T. P. et al., 2015. Regulated Eukaryotic DNA Replication Origin Firing with Purified Proteins. *Nature*. pp. 431-435.

Zhang et al., 2019. MiR-3150b-3p inhibits the progression of colorectal cancer cells via targeting GOLPH3. *Journal of Investigative Medicine*. DOI:10.1136.